Regional estimates of gross primary production applying the process-based model 3D-CMCC-FEM vs. multiple datasets

Running title:

Key words: Process-based forest model; gross primary production; climate change; national forest inventory; Mediterranean region;

Authors:

D. Dalmonech [1,2], M. Chiesi[3], G. Chirici[4], L. Fibbi[3], F. Giannetti[4], G. Marano[5], C. Massari[6], A. Nolè[7], E.Vangi[1], J. Xiao[8], A. Collalti[1,2,9]

[1] Forest Modelling Laboratory, Institute for Agriculture and Forestry Systems in the Mediterranean, National Research Council of Italy (CNR-ISAFOM), Via Madonna Alta 128, 06128 Perugia, Italy

[2] National Biodiversity Future Center (NBFC), 90133 Palermo, Italy

[3] National Research Council of Italy, Institute of BioEconomy, (CNR-IBE), via Madonna del Piano 10, 50019 Sesto Fiorentino, Italy

[4] GeoLab - Laboratory of Forest Geomatics, Dept. of Agriculture, Food, Environment and Forestry, Università degli Studi di Firenze, Via San Bonaventura 13, 50145 Firenze.

5 Forest Ecology, Institute of Terrestrial Ecosystems, Department of Environmental Systems Science, ETH Zurich, Zurich, Switzerland

[6] Research Institute for Geo-Hydrological Protection, National Research Council (CNR-IRPI), Via Madonna Alta 126, 06128 Perugia, Italy

[7] School of Agricultural, Forest, Food and Environmental Sciences University of Basilicata, Italy

[8] Earth Systems Research Center, Institute for the Study of Earth, Oceans, and Space, University of New Hampshire, Durham, NH 03824, USA

[9] Department of Agricultural and Forestry Sciences (UNITUS-DAFNE), Tuscia University of Viterbo, Via San Camillo de Lellis snc, 01100, Viterbo, Italy

Corresponding author: D.Dalmonech daniela.dalmonech@isafom.cnr.it

ORCID:

Dalmonech D.: 0000-0002-1932-5011

Chiesi M. : 0000-0003-3459-6693

Chirici G. : 0000-0002-0669-5726

Fibbi L. : 0000-0001-6985-6809

Giannetti F.: 0000-0002-4590-827X

Marano G.: 0000-0003-2600-984X

Massari C.:0000-0003-0983-1276

Nolè A. : 0000-0002-5144-3421

Vangi E.: 0000-0002-9772-2258

Collalti A.: 0000-0002-4980-8487

Key Points

1. We apply a process-based forest model on a regular grid at 1 km spatial resolution in a Mediterranean region.
2. Initial forest state is estimated using spatially explicit input data derived from national forest inventory data and remote sensing.
3. The model shows satisfactory performances in simulating the gross primary productivity fluxes, when compared to three independent multi-sources satellite-based observations.

Abstract

Process-based models (PBMs) offer the possibility to capture important spatial and temporal patterns of both carbon fluxes and stocks in forests, accounting for ecophysiological, climate, and geographical variability. For the first time, the stand scale process-based model 3D-CMCC-FEM is applied in a spatially explicit manner at 1 km spatial resolution in a

Mediterranean region in southern Italy. We developed a methodology to initialize the model that comprehends the use of spatial information derived from the integration of the national forest inventory data, remote sensing data, and regional forest maps to characterize structural features of the main forest species. Gross primary production (GPP) fluxes are simulated over the period 2005-2019 and the predictive capability of the model in simulating the carbon fluxes is evaluated by means of independent multiple data sources based on remote sensing products. We show that the model is able to reproduce most of the spatial and seasonal variability and patterns of the observed productivity, even at the species-level. These new very promising results open the possibility of using the 3D-CMCC-FEM to investigate the forests' behavior under climate and environmental variability over large areas in the future, across the highly variable ecological and bio-geographical heterogeneity of the Mediterranean region.

1. INTRODUCTION

Forest ecosystems absorb globally ~2 Gt of Carbon (C) stocking the carbon in their biomass and soil, thus acting as a net carbon sink. In Europe alone, forests ecosystems, which cover for about a 40%, currently act as a net carbon sink for 315 $MtCO_2eq$ and compensating for about 8% of EU-27's total greenhouse emissions (Verkerk et al., 2022).

However, adverse climate impacts such as heat waves and drought (Allen et al., 2015; D'Andrea et al., 2020, 2021; Schuldt et al., 2020) and increasing natural disturbance rates (Grünig et al., 2023; Patacca et al., 2023) are all stressors which have potentially significant effects on current and future forest dynamics, jeopardizing the European forest ecosystems functioning and their carbon mitigation potential under future climate change (Schuldt et al., 2020; Senf et al., 2020). This is particularly true across the Mediterranean region known as a climate change hotspot (Dubrovský et al., 2014; Noce et al., 2016), with projections

indicating a higher warming rate (Noto et al., 2022), decrease in precipitation in particular in the summer and a large increase in frequency and intensity of extreme events such heat waves and droughts (Dubrovský et al., 2014; Turco et al., 2017).

Nevertheless, ground data scarcity and short-term monitoring efforts still represent major challenges in studying the effects of climate change on forest dynamics in Mediterranean areas because are characterized by a large ecosystem heterogeneity and a biogeographically diverse structure shaped by human activity (Peñuelas et al., 2017; Gauquelin et al., 2018; Médail et al., 2019). In the context of climatic uncertainty and future trajectories of forest dynamics and impact of future climate, it is thus crucial in Mediterranean areas to provide large-scale forest monitoring and eventually prognose the state of forest ecosystems by means of analytical tools.

In this context, process based forest models (PBFMs) are developed and tested over a wide range of applications, because of their capability in simulating forest ecosystem long term dynamics (Bugmann & Seidl, 2022), carbon fluxes exchange and stocks (Chiesi et al., 2010; Reyer et al., 2014; Mahnken et al., 2022) under external environmental variability by accounting for population dynamics and inner physiological processes mechanistically (Maréchaux et al., 2021; Pretzsch et al., 2008). On the other side of the ledger, given the large amount of requested data for their initialization and parameterization, such detailed models are mostly run at a very local scale, i.e. site level (one hectare or a bit more), where high-quality/measured ancillary data to initialize the model and observed meteorology are available (e.g. Collalti et al., 2016; Suárez-Muñoz et al., 2023). Yet, initializing stand scale PBFMs from actual, measured forest state variables, or close to the observed states, rather than from equilibrium conditions, is the desirable option to implicitly take into account the climate and management history of the site, and to more realistically simulate the response of forest to climate change, and natural and anthropogenic disturbances (e.g. Pretzsch et al., 2008;

Kannenberg et al., 2020). Only recently, stand scale PBFMs were applied on a regular grid (see Sanchez-Ruiz et al., 2018; Minunno et al., 2019) or at several sites at the national level in central and northern Europe (Gutsch et al., 2018; Härkönen et al., 2019), with the only purpose of estimating aggregated carbon stocks and products at regional or country level.

However, stand scale PBFM represents versatile tools capable of simulating both carbon fluxes and stocks. Fluxes respond sensitively to climate variability operating at the daily to decadal time scales (e.g. Reyer, 2015; Gutsch et al., 2018; Collalti et al., 2018; Dalmonech et al., 2022) and can be considered a good proxy of the ecosystem physiological functionality in forests (Collalti et al., 2018; Chen et al., 2023a).

The objective of this study is thus to test the predictive capability of the biochemical, biophysical, process-based forest model 3D-CMCC-FEM (Collalti et al., 2014, 2016), on a regular grid at 1 km resolution to simulate gross primary production (GPP) at regional scale. As case study, the model was tested over one of the southernmost regions in Italy, the Basilicata Region. The ability to simulate the GPP flux is here considered because it is significantly influenced by meteorological and climate year-to-year variability (e.g. (Mahnken et al., 2022; Fernández-Martínez et al., 2023) and its seasonal variations in the Mediterranean areas are distinctively shaped by the atmospheric water demand and soil water availability in summer.

As most regions in the Mediterranean basin, Basilicata spans over a multitude of ecological, morphological and soil-type gradients and climate conditions, and the paucity of ancillary or ground data represents the main obstacle to PBFMs initialization and hence model application PBFMs at high resolution at these spatial scales. We simulate the GPP, initializing the model through the use of spatial information derived by integrating the national forest inventory data, remote sensing (RS) data and regional forest maps to characterize structural features of the main forest species and model results are evaluated against a portfolio of independent RS-

based data. The model-data agreement is presented and sources of uncertainties and challenges of applying a PBFMs by means of the presented modeling strategy are also discussed.

2. MATERIALS AND METHODS

2.1 STUDY AREA

The Basilicata region has a spatial extent of about 10,000 km^2 and is located in southern Italy (Figure 1). It is characterized by typical Mediterranean climate conditions with hot and dry summers and wet and mild winters. The region has been chosen to test the model in a complex biogeographic area with pronounced environmental gradients. The territory is characterized by about 47% of mountain areas represented by the Apennines Mountains, followed by hilly areas, about 45%, and then plain. Average annual precipitation varies between ~500 and ~2000 mm $year^{-1}$, mirroring the orographic complexity of the region and the proximities to the sea, with a west-to-east gradient from humid to dry sub-humid areas.

According to the last national forest inventory (INFC 2015), forest vegetation and other wooded lands occupy 392,412 ha, about 39% of the region. Deciduous species cover 54% of the forest area and are represented mainly by Quercus oak (*Q. cerris* L., *Q. ilex* L.), which dominated the hilly areas between 400 and 1200 m a.s.l., and European beech (*Fagus sylvatica* L.) the main species above 1000 m a.s.l. as reported in Figure 2a. Coniferous species are less abundant and are represented mainly by Pinus ssp (*P. halepensis* Mill., and *P. nigra* J.F. Arnold), used for reforestation purposes (Figure 2a).

2.2 THE PROCESS-BASED MODEL 3D-CMCC-FEM

The 3D-CMCC-FEM (*Three Dimensional – Couple Model Carbon Cycle – Forest Ecosystem Model*) is an eco–physiological, biogeochemical, biophysical process-based model which simulates the dynamic of carbon fluxes and its allocation through a cohort-structured forest stands (Collalti et al., 2014, 2018), providing detailed output at daily time scale of Carbon

fluxes and pools. The model simulates forest growth and structural development at varying environmental conditions and different climate, atmospheric CO_2 concentrations and forest management scenarios (Collalti et al., 2019; Dalmonech et al., 2022; Testolin et al., 2023).

The daily gross photosynthesis is simulated through the Farquhar–von Caemmerer–Berry biochemical model (Farquhar et al. 1980), modified for sun and shaded leaves (de Pury & Farquhar, 1997), and acclimated for temperature (Kattge & Knorr, 2007). The carbon allocation schemes are described extensively in Collalti et al. (2016, 2019, 2020) and Merganičová et al. (2019). Tree removal occurs via management (see Testolin et al., 2023) or by natural mortality. Self-thinning, age-related mortality, carbon starvation, and background mortality represent the different types of mortalities simulated by the model (Collalti et al., 2016). Soil hydrology is simulated by means of a one-soil layer with free drainage. The plant water availability in the model is thus modulated by the soil depth (i.e. rooting depth until which the water is uptaken to sustain leaf transpiration), because of the zero-dimensional soil model. Soil water stress operates on canopy exchange processes *via* stomatal and biochemical pathways (e.g. photosynthesis). An in-depth description of the model's underlying characteristics, effects of climate change and model parameter sensitivity and uncertainty, as well as model limitations, is reported in Collalti et al. (2019).

The model has been extensively evaluated at the site level and evaluated against measurements of carbon fluxes from the FLUXNET eddy covariance towers database and ancillary data. The evaluation has been carried out in the past over a broad spectrum of climate and species, however in sites mainly concentrated in central and northern Europe and at site-level (Collalti et al., 2016; Marconi et al., 2017; Dalmonech et al., 2022). In a recent inter-comparison study, the model was shown to be able to simulate C fluxes, e.g. GPP, and key structural variables, e.g. diameter, basal area, etc, with very good performance when compared to measured data and to other forest models (Mahnken et al., 2022).

2.3 FOREST DATA

The model requires the description of the forest structural characteristics i.e. diameter at breast height (DBH), tree height (H) and stand density (number of tree per hectare), in order to be initialized and to run the simulations. To estimate average forest structure we used data from the second Italian national forest inventory (NFI) of the year 2005 (www.inventarioforestale.org), and a wall-to-wall map of basal area for the Italian territory. The NFI is based on a three-phase, systematic, unaligned sampling design with 1 x 1 km grid cells. In the first phase, 301,300 points were extracted and classified using aerial orthophotos into forest/non-forest categories. In the second phase, a field survey was carried out in a sub-sample of the first-phase points falling in the forest category, to collect qualitative information such as forest type, management, and property. Finally, in the third phase, for a sub-sample of 6782 points extracted from the second-phase points, a dendrometric survey was carried out for circular plots of a 13 m radius. All tree stems with DBH of at least 2.5 cm were callipered, and for a subsample, height was measured.

A wall-to-wall map of the forest basal area at a 23 m spatial resolution, was developed following the procedure presented by (Chirici et al., 2020; Vangi et al., 2021; Giannetti et al., 2022). This map consists of random forest predictions of basal area per hectare for all 23 m spatial resolution forest pixels. The model was trained using NFI plot-level data and Landsat and other RS datasets as predictors, including climate information such as minimum, mean, and maximum temperature, and daily precipitations from the E-OBS dataset. The model fitting and tuning steps were carried out using the '*randomForest'* package in the statistical software R 4.0.5 (Liaw & Wiener, 2002)(https://www.r-pr oject.org, accessed on: May 2nd, 2023). More information about these steps can be found in Chirici et al. (2020), Giannetti et al. (2022) and Vangi et al. (2021). The pixel-level estimations of the basal area range between

5 and 43 m^2 ha^{-1} with a mean value of 12 m^2 ha^{-1}, that is in line with the range reported in the context of NFI for the field plots data estimation.

2.4 FORCING AND SOIL DATA

The model is forced with daily maximum (Tmax, °C) and minimum (Tmin, °C) air temperatures, precipitation (P, mm day^{-1}), downward short-wave radiation at the surface (SW MJ m^{-2} day^{-1}) and relative humidity (RH, %). Climate data for the period 2005-2019 were retrieved from the E-OBS v.23.1e gridded dataset (Cornes et al., 2018). The E-OBS gridded dataset is derived through interpolation of the ECA&D (European Climate Assessment & Data http://eca.knmi.nl/) station data. The station dataset comprises a network of more than 2000 termo-pluviometric stations, with the highest station in northern and central Europe and lower density in the Mediterranean, Northern Scandinavia and Eastern Europe. The E-OBS dataset is derived through a three-stage process (Haylock et al., 2008), which brings it to different resolutions and grids. In this analysis, we used the 0.1◦ regular latitude–longitude grid. The E-OBS dataset has already been used in environmental impact studies (e.g. (Rita et al., 2020), climate scenarios bias correction (Dosio & Paruolo, 2011; Rojas et al., 2011) and benchmark activities (Moreno & Hasenauer, 2016; Herrera et al., 2019; Lorenz et al., 2019; Massari et al., 2020).

All the physical variables were bilinearly interpolated to the regional grid at 1 km resolution and re-projected onto the UTM-33 Mercator using the nearest neighbor sampling method. The temperature forcing data were corrected for the topographic effect by applying a lapse rate correction based on elevation differences between the E-OBS reference elevation and the simulation elevation grid. The latter was extracted from the TINITALY project, a national digital elevation model of Italy at 10 m resolution (Tarquini et al., 2009). The lapse rate

229 estimates of –5 °C/km for Tmax and –3 °C/km for Tmin, were derived from termo-
230 pluviometric ground station measurements over an elevation transect in the Basilicata region.

231 The model was forced by global annual atmospheric CO_2 concentrations from Dlugokencky
232 and Tans (https://www.esrl.noaa.gov/gmd/ccgg/trends/), covering in total the years 2005-
233 2019.

234 The model requires soil depth as well as soil texture for each grid cell. As a proxy of soil
235 depth, we used the estimated depth available to root from the European Soil Database Derived
236 Data product ESBD v2 (Hiederer, 2013) provided at 1 km resolution. The lower depth value
237 of each class of the map was attributed, and a maximum of 1 m for the rooting depth was set.
238 This boundary value can be considered a good approximation for European forests (Schenk &
239 Jackson, 2005). Soil texture as a percentage of clay, silt, and sand was estimated from the
240 pedological map of the region (year 2005).

241 **2.5 MODEL SIMULATIONS**

242 **2.5.1 MODEL INITIALIZATION**

243 The 3D-CMCC-FEM model (v.5.6) was applied on a regular grid at 1 km spatial resolution
244 over the selected region to simulate the forest carbon dynamic starting in January 2005 until
245 December 2019. The model requires the description of the actual forest characteristics in
246 order to be initialized.

247 The initial forest state was set according to a simplified configuration of the forest
248 aboveground structural complexity, i.e. for each grid cell of the target domain, we determined
249 the dominant forest species and estimated the average structural data: the average tree
250 diameter at breast height (DBH), average tree height (H), stand density and average age class.

251 The following parameterized key species were considered: European beech (*Fagus sylvatica*
252 L.), Black pine (*Pinus nigra* J.F. Arnold), Sweet chestnut (*Castanea sativa* Mill.), Turkey oak

(*Quercus cerris* L.), Aleppo pine (*Pinus halepensis* Mill.) and Holm oak (*Quercus ilex* L.) as representative of the most common forest types in the study area. Maquis and other minor forest species are not parameterized or simulated in the model and thus were excluded from the simulation domain. For each grid cell, we defined the dominant forest species as the one covering the highest forest fraction to provide a 1 km resolution map (Figure 2a), resulting in a total covered area of ~2800 km^2, corresponding, overall, to ~78 % of the regional forested area.

Forest average structural data, i.e. DBH, and stand density were estimated for the year 2005 from the wall-to-wall basal area map and the NFI 2005 data. Tree density data of the NFI elementary plots were used to provide a representative estimate the forest density in each grid cells. To do so we zonally averaged the density data according to the model forest species classes and the Italian 'mountain communities' units (Amato et al., 2008). These Italian administrative units are characterized by a certain degree of geographical homogeneity and their forest management and protection is delegated by the Regions to the local administrations. The information of tree density was then used in combination with the basal area data from the wall-to-wall map, to calculate an average DBH and the data were resampled onto the target grid to provide a 1 km resolution DBH map for each dominant species (data not shown).

To be consistent with the model processing, the average tree height of the stand was calculated from DBH by applying the calibrated Chapmann-Richard equation (Richards, 1959) for each forest class.

From these structural variables, i.e. DBH and H, the model self–initializes at the beginning of simulations the other carbon state variables, i.e. leaf, stem, branches, coarse root, reserves, carbon pools, according to species–specific allometric relationships.

The regional forest map of Basilicata provided a *stratum*, which describes the development stage of the aboveground vegetation forest and type of forest (Corona, 2008). This information was used to estimate the average age class for each dominant species in each grid cell (Table S1, Supplementary material).

Where needed, the geographic information were re-projected, to a common UTM zone 33 North coordinate reference system under the WGS84 datum and then resampled onto the simulation grid. The main data analyses were performed using the computing language *R* (R Core Team 2021). Key packages used for data preprocessing included '*terra'* (Hijmans, R. J., Bivand, R., Forner, K., Ooms, J., Pebesma, E., & Sumner, 2022) and '*rgdal'* (Sumner & Hijmans, 2023)

2.5.2 SIMULATIONS SETTINGS

Due to the relatively short time period covered by the simulations, i.e. 2005-2019, we did not consider any change in dominant species. For the same reason and because of the spatial resolution, a constant thinning rate implemented each year was considered as the only silvicultural intervention. The thinning rate was derived from the forest management guidelines of the region as set to a yearly removal rate of 1%, corresponding to ~20% of biomass removed in 20 years. Forests in protected areas of the Natura 2000 network of the region are characterized by lower disturbance extension compared to the other forested areas according to the disturbance maps (Francini et al., 2021), and are assumed to be interested by a lower level of tree fellings. For simplicity we assumed thus fellings in these forests are mainly caused by natural and background mortality alone. Grid cells interested by fire events over the period 2005-2019, were identified using the national dataset of burnt areas from forest fires, produced by the Italian Forest Service (Comando Unità Forestali, Ambientali e Agroalimentari of Carabinieri). This dataset is acquired through a ground survey using Global Navigation Satellite System receiver (GNSS) and is available from 2005 to 2019. Grid cells

interested by fire were excluded from the analysis as the model does not simulate extended natural disturbances (i.e. fire and pests). No land use change is assumed in the simulation period.

2.6 GPP MODEL COMPARISON AT REGIONAL SCALE

Datasets based on RS data (or modeled by forcing with remote sensed data) are the most suitable candidate to assess the overall model capability at reproducing the GPP fluxes over large areas, due to their continuous spatial and temporal coverage. In order to make a more complete and comprehensive agreement assessment, we selected gridded GPP estimates from different sources as reference datasets, which are:

GOSIF-GPP

The GOSIF-GPP dataset (Li & Xiao, 2019b) is a recently developed GPP product that is based on the global OCO-2 based SIF product (GOSIF)(Li & Xiao, 2019a). The GOSIF setup combines in a data-driven approach the remotely sensed sun-induced fluorescence (SIF), observed by the Orbiting Carbon Observatory-2 (OCO-2), the enhanced vegetation index (EVI) from the Moderate Resolution Imaging Spectroradiometer (MODIS) satellite data, meteorological data, i.e. photosynthetically active radiation (PAR), vapor pressure deficit (VPD), and air temperature obtained from the NASA reanalysis MERRA-2 data set to return a gridded SIF dataset (Li & Xiao, 2019a). Established relationships between the original OCO-2 SIF and flux tower GPP (Li et al., 2018; Xiao et al., 2019) were then used to provide a fine resolution GPP dataset at 0.05 degree for the years 2000-2022. For the model-data comparison in this study we used the monthly and annually aggregated ensemble mean of eight different GPP estimates resulting from different GPP-SIF relationships, (http://globalecology.unhedu). The estimates were bilinearly interpolated to the target grid.

CFIX

The CFIX dataset provides gridded GPP covering Italy. The estimates are obtained combining meteorological and remotely sensed data within a Light Use Efficiency modeling approach (Maselli et al., 2006; Veroustraete et al., 2002). The original model version was further modified to simulate the GPP of water-limited, Mediterranean forest ecosystems by (Maselli et al., 2009), who introduced a short-term water stress factor based on daily meteorological data. In particular, the authors utilized the 1-km normalized difference vegetation index (NDVI) from the Spot-VEGETATION imagery to linearly retrieve the fraction of absorbed photosynthetically active radiation, and the downscaled E-OBS meteorological data (both air temperature and precipitation)(Maselli et al., 2012; Fibbi et al., 2016) to retrieve the GPP of all Italian forests at 1-km spatial resolution. The same model was also applied using higher spatial resolution NDVI data taken by the MODIS Terra and Aqua sensors (Chiesi et al., 2011; Maselli et al., 2013)**.**The accuracy of the product was assessed by comparison to Eddy-Covariance GPP data collected at several EC sites spread over the Italian peninsula and for different forest types, showing satisfactory performances (Maselli et al., 2009). The currently utilized product, hereinafter referred to CFIX-GPP, provides forest GPP estimates at 1 km spatial resolution aggregated on a monthly time step, over the years 2005-2013. For the current study, the original dataset is projected from the original UTM 32 Nord projection to UTM 33 Nord by means of the nearest neighbor method.

FLUXCOM

The FLUXCOM dataset is an upscaled product derived from different Machine Learning-based approaches (ML) combining data from the FLUXNET network of eddy covariance towers with RS and meteorological data as predictors (Jung et al., 2019; Pastorello et al., 2020). RS land products at 8-day resolution from the MODIS instrument, such as EVI,

fAPAR, and the land surface temperature, were used as predictors in the FLUXCOM-RS statistical framework. The FLUXCOM-RS+METEO setup provides instead gridded GPP estimates based on the MODIS-RS data and different global climate input data (see Jung et al. 2019 for a thorough description of the FLUXCOM products). However, for this study, the FLUXCOM-RS dataset was selected because of its finer resolution, 0.083 degree, in order to better deal with the complex topography of the region under study and to reduce potential inconsistencies that would stem from the use of a climate-forcing in the RS-METEO version different than the one used to force the forest model.

The FLUXCOM-RS dataset, hereinafter simply referred to as FLUXCOM-GPP, has been widely used as a reference dataset in several inter-comparison studies with both model and other reference datasets (O'Sullivan et al., 2020; Wang et al., 2021; Y. Zhang & Ye, 2021). The selected estimates dataset is provided as monthly data covering the period 2000-2015 (www.fluxcom.org). The ensemble mean of monthly data computed from multiple ML algorithms was used and bilinearly interpolated over the region at 0.01-degree resolution and resampled to the target grid.

The analysis on annual GPP and mean seasonal cycle focused on the common years of the model simulations and the selected reference datasets, hence 2005-2013 and the agreement assessment was carried out on the monthly output of the model.

For each grid cell the multiyear average annual GPP for data and model was computed and the spatial agreement was assessed by means of the SPAtial EFficiency metric (SPAEF) in eq.1). This is an integrated evaluation index which considers the spatial correlation R, the fraction of the coefficient of variation $\beta = (\sigma_{sim}/\mu_{sim})/(\sigma_{obs}/\mu_{obs})$ and the model-data histogram intersection $\gamma = \sum_{j=1}^{n} \min(K_j/L_j)/\sum_{j=1}^{n} K$, where n is the number of bins in the histogram and K and L are the histogram for observed and simulated data (Koch et al., 2018) SPAEF is equal to 1 in the case of perfect match.

$$SPAEF = 1 - \sqrt{(R-1)^2 + (\beta-1)^2 + (\gamma-1)^2} \qquad \text{Eq. 1)}$$

The evaluation metric list includes additionally the root mean square error (RMSE) and the fractional mean bias (FBM)(Janssen & Heuberger, 1995). The analyses for the mean seasonal cycle were carried out at the cell level and the squared correlation R^2 between the modeled and the reference mean seasonal cycle was computed, as in Jung et al. (2019).

The ability of the model to capture the interannual variability of the spring (March, April, May) and summer (June, July, August) aggregated GPP value, was assessed with the correlation coefficient R, at grid-cell level, which returns the direction of the correlation i.e. model-data correspondence of the sign of year to year variability. We compared the model to the only dataset (GOSIF-GPP) with data over the years 2005-2019. The temporal aggregated level and the less stringent metric is justified by the higher uncertainties in interannual variability across remote-sensing-based datasets (e.g. Butterfield et al., 2020). Anomalies were calculated for the model and data by first removing the long-term linear trend, to remove any demographic, forest development, or age effects, for the period 2005-2019, and normalized by their standard deviation.

To diagnose how well the modeled summer GPP anomalies follow the meteorological variability during the vegetative season prior to August, compared to the reference dataset, we used the Standardized Precipitation Evaporation Index, SPEI (Vicente-Serrano et al., 2010). This is a multi-scalar meteorological drought index based on a statistical transformation of the climatic water balance, i.e. precipitation *minus* potential evapotranspiration. We computed the SPEI using the simplistic Hargreaves equations for the potential evapotranspiration calculation and considered different time scales, with the aim to cover the growing season period before the month of August. Following a similar approach as in Mahnken et al. (2022), we regressed the residuals of the model-dataset anomalies differences against the SPEI values

as the predictor, and the slope of the linear regression computed. Values of the slope close to 0 indicate that the model shows a GPP-sensitivity to SPEI like the reference dataset.

3 RESULTS

3.1 MEAN ANNUAL GPP ESTIMATES

The simulated average annual GPP fluxes for the period 2005-2013 are shown in Figure 2b, with values ranging from ~600 up to 2200 $gCm^{-2}y^{-1}$. Modeled GPP follow a west-east gradient with higher productivity over the western side of the region in correspondence with the more humid areas and the more productive beech-dominated areas; the forested areas over the plain zones are mainly dominated by Mediterranean pine species, which show the lowest GPP (Figure 2a,b). Relative biases between the model and the GOSIF-GPP dataset are within ±15% in large areas of the region (Figure 3a-d). Nevertheless, a west-east gradient in the differences is apparent at the regional level (Figure 3a). The observed GPP-bias seems coherent with the bias detected when comparing the modeled annual maximum Leaf Area Index to the MODIS product (Figure S.2.1 a-c in Supplementary Material). This coherency is detected only when comparing the model to the GOSIF-GPP dataset. A similar low average relative GPP-bias is also found when considering the CFIX-GPP dataset (Figure 3b-d). However, differently than GOSIF-GPP, the model generally tends to slightly underestimates GPP when CFIX-GPP is lower than ~1500 $gCm^{-2}y^{-1}$ and to slightly overestimate GPP when GPP is higher than ~1500 $gCm^{-2}y^{-1}$ as shown in Fig. 4b). Model differences to the FLUXCOM-GPP estimates reveal instead a systematic positive bias over the entire region at exception of the eastern plain areas where the bias is narrow and closer to 15% (Figure 3c-d, Fig. 4c). The RMSE of the average simulated GPP is 232.8 $gCm^{-2}y^{-1}$for GOSIF-GPP, 221.9 $gCm^{-2}y^{-1}$for CFIX-GPP and 439.5 $gCm^{-2}y^{-1}$FLUXCOM-GPP. All performance metrics are reported in Table 1. The fractional mean bias, which provides a measure of the tendency for

over or under-prediction (i.e. positive or negative values) is –0.05, 0.0 and 0.31 for GOSIF-GPP, CFIX-GPP and FLUXCOM-GPP, respectively.

When considering the differences aggregated according to forest species, the positive bias between model and CFIX-GPP and FLUXCOM-GPP is particularly evident over beech dominated forests (Figure 4b,c and S2.2a in Supplementary Material). The detected geographical bias between the modeled GPP values and the GOSIF-GPP estimates mainly interests the oak dominated forests as shown in Figure 4a and S2.2 in Supplementary Material. Modeled differences to datasets are lower and close on average to 0 in areas dominated by Mediterranean pines, when the model is compared to GOSIF-GPP and FLUXCOM-GPP data (Figure 4a-c, S2.2a in Supplementary Material), while there is a negative bias when comparing the model results to the CFIX-GPP estimates (Figure 4b and 2.2a).

The model shows generally a good capability to simulate the spatial variability of the annual GPP, with spatial pattern of the modeled GPP which better mirrors that of the GOSIF-GPP with a correlation value of R = 0.79, compared to CFIX-GPP and FLUXCOM-GPP datasets showing correlations values of R = 0.59 and R = 0.68, respectively (Figure 4a-c, Table 1). The better correspondence between the model and the GOSIF- and FLUXCOM-GPP datasets is also mirrored by the metric β, the fraction of the coefficient of variation, with values of 0.81 and 1.1 respectively, against a value of 1.97 when comparing to the CFIX-GPP dataset. The better agreement is also found in the qualitative relationship between the Basal Area for each dominant forest class in each grid cell at 2005 and the 2005-2015 average annual GPP (Figure S2.3 in the Supplementary Material). However the model showed a slightly better histogram match when compared to the CFIX-GPP dataset, with a value of γ of 0.84.

Summarizing the results with the SPEAF metric, the GOSIF-GPP is the model with the highest score, i.e. closer to 1 (Figure 4, Tab.1).

3.2 MEAN SEASONAL CYCLE

Generally, the model shows very high correlations of the simulated mean seasonal cycle of GPP with all the reference datasets, with median R^2 = 0.82, R^2 = 0.9 and R^2 = 0.85 when compared to GOSIF-GPP, CFIX-GPP and FLUXCOM-GPP respectively (Figures 5a-d, Table 1). High correlation values are reported in particular at higher altitude (Figure1, 5a-c). Better performances across all reference datasets, are achieved in areas covered by beech and oaks species, with the highest model-data coherency when comparing to CFIX-GPP estimates. On the other hand, the lowest performances were returned for Aleppo pine forests, showing poorer correlation values (Figure S2.2b, S2.4 in Supplementary Material). The 3D-CMCC-FEM tends to anticipate the onset of the spring GPP increase when compared to GOSIF-GPP and FLUXCOM-GPP, especially for evergreen species (Figure S2.4 in Supplementary Material).

3.3 INTERANNUAL VARIABILIY

In this section, we show the ability of the model to track the GPP variability in spring and summer and to capture the response of summer GPP to spring and summer meteorological conditions. The analyses focus on the GPP anomaly values, and the results are presented comparing the model to the GOSIF-GPP dataset, as it is the longest record among the three data streams (Figure 6). The correlation between modeled and reference IAV of spring GPP anomalies are positive over large areas (Figure. 6a), however, the model shows low-performance metrics with a median R-value of 0.15 (Table1). Negative correlations appear clustered on the plain areas. No significant differences in performance emerge across reference datasets when considering the period 2005-2013 (data not shown). Summer anomalies are better captured by the model with an average spatial correlation of R = 0.53 and

values that are most significant in the western and hill-mountains areas of the region (Figure 6b).

The SPEI drought index helps highlight periods of wetter or drier conditions with respect to the long-term mean conditions. A time scale of 5 months in the SPEI index is considered (SPEI5), as it is the one where the association between SPEI and summer GPP in the reference data is stronger (data not shown). The same temporal scale was used for the entire region, without considering, for example, any potential lagged effects. We empirically estimate if the model and data differ in the summer GPP sensitivity toward interannual variation in SPEI5 by computing the slope of the regression line between differences in GPP anomalies and the drought index SPEI5. Spring anomalies are not considered here due to the poor correlations between the model and data shown in Figure 6.a. In large areas of the region, which are characterized by higher summer-GPP anomalies correlations, the slope is not significantly different from 0 (Figure 6b, 7). Only in clustered areas, e.g. the center, of the region the slope is positive and significant.

1. DISCUSSION

In this study, we ran the 3D-CMCC-FEM spatial explicitly over a Mediterranean area characterized by significant bio-geographical and climatological heterogeneity. Initializing the forest structure from ground data and basal area maps allows having a more realistic initial state of the carbon pool and forest structure, reducing, thus, uncertainties in the initial pools which might translate into significant differences in the carbon fluxes (Carvalhais et al., 2008, 2010; Lindeskog et al., 2021). The calibration of the allometric equations, to which the model is sensitive (Collalti et al., 2019), sets a constraint on the modeled growing biomass trends, which in turn influences the simulated GPP *via* the amount of sapwood. By means of the use of the basal area map to build the forest characteristics in the first year of simulation, the

model is able to retain part of the spatial information of initial aboveground biomass and average forests structure, contributing, for instance, to the very good spatial correlations of the modeled annual GPP with data. While aggregating basal area data at the 1 km resolution might reduce random uncertainties in basal area, additional uncertainty might stem from the tree density data, which is less constrained. Yet, performed tests (not shown here) indicate no significant sensitivity of the simulated GPP to stand density.

Despite the very simple initial forest setup, model performances in simulating the gross primary production – when compared to other large scale and independent data – are shown to be generally satisfactory over different temporal scales. Residual data-model differences across datasets emerging from the comparison analyses are attributable to several sources of uncertainties related to the reference datasets, the model, and the forcing.

5.1 Reference dataset uncertainties

The 3D-CMCC-FEM model shows simulated annual fluxes closer to the GOSIF and CFIX–GPP estimates than the FLUXCOM-GPP values, with better spatial correspondence to the GOSIF-GPP estimates. The modeled GPP is larger than the FLUXCOM-GPP data, usually considered a benchmark dataset, a result which is common to other process ecosystems and dynamic vegetation models (Jung et al., 2020; Y. Zhang & Ye, 2021). Recent studies found that the GPP may be underestimated in the FLUXCOM-GPP in temperate areas (e.g. Bacour et al., 2019; Norton et al., 2019; Wild et al., 2022). FLUXCOM-GPP is an upscaled product of the local EC-tower GPP estimates, and its accuracy relies also on the capability to sample in the entire climate-vegetation space (Jung et al., 2020). The GOSIF-GPP and the CFIX-GPP datasets instead have the advantage of having a finer spatial resolution and, thus, contain more information, with the GOSIF having a globally higher continuous coverage *via* the original SIF data. On the other hand, uncertainties in the relationship between GPP and SIF still

remain (Wohlfahrt et al., 2018; Bacour et al., 2019; Chen et al., 2021) and comparison studies showed that the GOSIF-GPP might overestimate the GPP values in temperate broadleaved forests (Qiu et al., 2020). Yet the SIF data from RS remain one of the best proxies for photosynthesis over large areas to date (Sun et al., 2017; Li & Xiao, 2019a), making the GOSIF-GPP estimates more robust estimates compared to both CFIX-GPP and FLUXCOM-GPP. Differences in the list of predictors used in the data-driven datasets, i.e. meteorological drivers or land cover used to drive the GOSIF-GPP and CFIX-GPP datasets, might additionally contribute to explain the model-data differences.

5.2 Model-related uncertainties

The simulated values of GPP in beech-dominated forests are, on average higher than the three reference dataset, with simulated values in some areas larger than 2000 $gCm^{-2}year^{-1}$. However these values are overestimated as observed average annual values of GPP in a beech forest in central Italy, a monitoring site with fluxes measured by means of the eddy covariance technique, are in the order of 1600 gC $m^{-2}year^{-1}$ with range between ~ 550 and 2500 $gCm^{-2}year^{-1}$ (Reyer et al., 2020) . When applied in the same beech forest, the model was shown to be able to simulate the observed range of GPP (Mahnken et al., 2022), indicating how the source of the observed significant bias might be attributable to uncertainties stemming from the up-scaling procedure and affecting the medium to higher elevation areas. Aggregated simulated values for the deciduous oaks are indeed more comparable to EC-estimates in a site in central Italy (Roccarespampani, Tedeschi et al., 2006; www.fluxnet.com) with annual values of the order of 1600 $gCm^{-2}year^{-1}$for model and observations.

The seasonal cycle of GPP describes the seasonal pattern of carbon gross assimilation by plants and the beginning and end of the growing season for the deciduous forests. For two out of the three datasets used here the 3D-CMCC-FEM might simulate a slightly earlier beginning

of the growing season (e.g. for chestnut). This might be partially attributable to the budburst parameterization, which is based on the Thermic sum and the growing degree days metric and a trigger for the beginning of leaf flushing. Such a parameter is kept constant (as in many other models, see Peano et al., 2019; Peaucelle et al., 2019), to limit the model's number of parameters, as a species-specific parameter, irrespective of any local climatological adjustment . The seasonality of the GPP in the evergreen species is instead shaped by the direct environmental effect on the photosynthetic process at a seasonal time scale, suggesting that the model-data differences might be attributable to bias in the meteorological forcing (section 5.3) or in other physiological parameters adopted. Indeed, model ecophysiological parameter values are derived from the scientific literature, yet not calibrated for the specific site or regions, in order to allow the model general applicability as reported in Mahnken et al. (2022).

To capture the summer GPP sensitivity to hydrological variability, i.e. wetter or drier conditions than the mean, we use a simple GPP-SPEI diagnostics. The model was first shown to be able to depict the interannual variability of the summer signal over a large extent, variability which is the most prominent feature in Mediterranean areas. As a matter of fact, in a previous study (see Collalti et al. 2016) was shown how at site level, in beech and coniferous forests, showing to be sufficiently able to return the sign of year to year variability of the annual signal. Yet interannual variability is the most uncertain signal event when comparing different database (see for instance summer anomalies in Figure S3 in the supplementary material).

In large areas of the region, the model and the reference dataset have a similar *response* in terms of GPP-SPEI5, as the residuals do not change with the SPEI. Yet, in some areas, a too-strong model response to SPEI also emerges, indicating that the model has a higher summer GPP-response to negative SPEI5 (i.e. drier conditions) compared to the reference dataset. In

particular, results indicate a higher modeled sensitivity of GPP to SPEI for oaks-dominated forests clustered on higher elevations. Oak's species are known to be an isohydric species, i.e. they weakly regulate stomatal openness under drought conditions and are more resilient to drought (Ripullone et al., 2020; Castellaneta et al., 2022), and it is possible that the high sensitivity of GPP to SPEI in the model is a result either of a too strong control of VPD on stomatal conductance (Grossiord et al., 2020) or a too strong soil moisture control on the photosynthetic process, shaped by the modeled soil water availability (Crow et al., 2020; Fang et al., 2021). However, site-level studies showed how the 3D-CMCC-FEM model realistically simulates the response of GPP to atmospheric VPD and temperature, at least at the site level (Mahneken et al. 2022). In the model soil hydrology is simulated *via* a single-layer bucket model and this might be another factor contributing to the stronger than observed response, as it has been shown as overall that the majority of models with a soil bucket hydrology tend to limit GPP more than models with other soil conceptual e.g. multilayered schemes (Hanson et al., 2004). One potential additional explanation to the modeled stronger GPP sensitivity to SPEI, would be the detected, although the narrow, earlier onset of the growing season in the model compared to the GOSIF-GPP dataset. In fact, leaf development not only drives how earlier or later the uptake of carbon from the atmosphere starts in the season, but also how earlier/later other processes, such as the leaf transpiration occurs in spring, potentially affecting the summer GPP response (e.g. Peano et al., 2019; Bastos et al., 2021; Chen et al., 2023b).

5.3 **Forcing uncertainties**

Low accuracy in the reconstructed meteorological forcing (see Bandhauer, 2021) might play an important role in impact studies that are conducted at high spatial resolution. The impact of the meteorological datasets used in data-driven and PBFMs was already shown to be

important to accurately simulate the GPP (e.g. Wu et al., 2017; Zhang et al., 2022). The 3D-CMCC-FEM was shown to be able to simulate GPP closer to observations at the site level in central and northern Europe, where the downscaling and bias correction of the modeled climate was facilitated by the local geography (see Collalti et al., 2018).

Potential positive biases in the original E-OBS temperature dataset, the accuracy of relies on the termopluviometric stations, might translate into too high average temperature at higher elevations where the temperature should be a limiting factor, partially explaining the high modeled GPP values in beech forests. Beech in the Italian Apennine Mountain regions represents, in fact, the upper limit of forest vegetation. Other studies (J. Fang & Lechowicz, 2006; Marchand et al., 2023) additionally showed that the most limiting factor for the presence and growth of the beech in Europe is, indeed, temperature,

Spatial biases in the modeled annual values of GPP emerge in this study, which cannot be explained by uncertainties in the modeling setup alone. When the model is applied spatially in a Mediterranean area with orographic and geographical complexity, the capability of the meteorological dataset to retain the spatial and temporal structure of precipitation might have important effects in modulating the modeled spatial and temporal GPP variability, and this will be the object of further investigation.

The last source of uncertainties in the data-model error might stem from the soil characteristics and, in particular, the soil depth. The dataset used in the analyses as a proxy of depth available to root does not show any spatial variability, e.g. with elevation, which is not realistic considering the topography and plasticity of plants roots (Fan et al., 2017; Stocker et al., 2023). The model at this scale of application would benefit from coupling with more advanced hydrological scheme or a soil depth parameterization, to better couple the vegetation with the effective soil water availability (Kollet & Maxwell, 2008; Niu et al., 2011)

or from soil moisture assimilation from remote sensing products (Kumar et al., 2014; Crow et al., 2020).

5.4 **LIMITATION AND FURTHER CONSIDERATIONS**

The satellite-based datasets capture the fluxes embedding the entire sub-grid variability, including the contribution of the vegetation not simulated by the model (e.g. crop, *maquis* and understory), in particular in areas where the forest cover is indeed low because of low stand density, such as in the plain areas of the region under study or in high soil degraded areas. Spatial scale mismatch between data and models may explain, thus, likely part of the low performances in some areas of the region or in spring. In addition, contrarily to the PBFM, the remote sensing based datasets are not designed to capture the different response of tree species to climate or the CO_2 fertilization effect, contributing to the discrepancies between reference data and model. Higher resolution reference datasets might be taken into consideration, however, at the expense of a shorter record length or lower accuracy in the satellite time series.

We did not consider the land use change and the model does not simulate any spatial interaction from neighboring grid cells, not allowing for example simulating forest expansion. We additionally aggregated the forest species according to macro classes, hence neglecting intra-specific differences, if any. However, we needed compromising input-model requirements, including parameters, to keep simulations and calculations feasible, and at the same time aim at tracking the forest response to environmental stress and climate variability. In particular, at the spatial resolution of the study, we were more interested in capturing trends in the key carbon variables than the finest sub-grid variability within the forest ecosystem.

No Nitrogen cycle is included, however, the precipitation is commonly identified as the main limiting factor for photosynthesis in Mediterranean areas (DeMarco et al., 2022).

5 CONCLUSIONS AND OUTLOOK

PBFMs offer a complementary tool to ground forest inventory networks and satellite-based records in monitoring the climate change impact and other disturbances on forests, tracking forest carbon dynamics and simulating potentially many other variables which are otherwise difficult to measure extensively or monitor continuously.

In this work, we applied for the first time the biogeochemical, biophysical, process–based model 3D-CMCC-FEM on a regular grid to simulate the gross primary production over a large area. This case study offered the possibility to test the model behavior directly at a regional scale under a typical Mediterranean climate. In spite of the simplified initial forest setup and the underlined source of uncertainties, the model was shown capable to capture the main features of the reference datasets. Further tests are needed, yet the very promising results open the possibility of using the PBFMs to investigate the spatio-temporal dynamics of forest growth over larger spatial scales and under drought conditions and future scenarios, shaped by the spatial climatic and ecological heterogeneity such as in the Mediterranean areas.

AUTHOR CONTRIBUTION

Daniela Dalmonech: Conceptualization, Data curation, Formal analysis, Investigation, Methodology, Resources, Software, Validation, Visualization, Writing - original draft. . **Gherardo Chirici, Francesca Giannetti** and **Elia Vangi:** Resources, Writing - review & editing. **Jingfend Xiao**: Resources, Writing - review & editing ; **Marta Chiesi** and **Luca Fibbi:** Resources, Writing - review & editing**. Gina Marano:** Software, review & editing **Christian Massari:** Writing - review & editing. **Angelo Nole**: Resources, Writing - review & editing **Alessio Collalti**: Conceptualization, writing - review & editing.

AKNOWLEDGMENT

The work was carried out in the framework of the project 'Advanced EO Technologies for studying Climate Change impacts on the environment – OT4CLIMA' (D.D. 2261 - 6.9.2018, PON R&I 2014–2020 and FSC). This work has been partially supported by MIUR Project (PRIN 2020) "Unraveling interactions between WATER and carbon cycles during drought and their impact on water resources and forest and grassland ecosySTEMs in the Mediterranean climate (WATERSTEM)"(Project number: 20202WF53Z), "WAFER" at CNR (Consiglio Nazionale delle Ricerche) and D.D., E.V., A.C. were supported by PRIN 2020 (cod 2020E52THS) - Research Projects of National Relevance funded by the Italian Ministry of University and Research entitled: "Multi-scale observations to predict Forest response to pollution and climate change" (MULTIFOR, project number 2020E52THS). D.D., E.V., A.C. acknowledge also funding by the project OptForEU H2020 research and innovation programme under grant agree-ment No. 101060554.

D.D. thanks Carlo Trotta for valuable discussions about tree allometric relationships and thanks Matteo Willeit for providing comments on a previous draft of the manuscript. We acknowledge the E-OBS dataset from the EU-FP6 project UERRA (https://www.uerra.eu) and the Copernicus Climate Change Service, and the data providers in the ECA&D project (https://www.ecad.eu)". The FLUXCOM products were obtained from the Data Portal at https://www.fluxcom.org/.

The 3D-CMCC-FEM model code version 5.6 is publicly available and can be found on the GitHub platform at: https://github.com/Forest-Modelling-Lab/3D-CMCC-FEM). Correspondence and requests for additional materials should be addressed to the corresponding author.

References

Allen, C. D., Breshears, D. D., & McDowell, N. G. (2015). On underestimation of global vulnerability to tree mortality and forest die-off from hotter drought in the Anthropocene. *Ecosphere*, *6*(8), 1–55. https://doi.org/10.1890/ES15-00203.1

Amato, V., Lanza, G. G., Foresta, D. La, & Simonetti, L. (2008). *Comunità montane . Soggetti propulsori dello sviluppo o enti inefficaci ?*

Bacour, C., Maignan, F., MacBean, N., Porcar-Castell, A., Flexas, J., Frankenberg, C., Peylin, P., Chevallier, F., Vuichard, N., & Bastrikov, V. (2019). Improving Estimates of Gross Primary Productivity by Assimilating Solar-Induced Fluorescence Satellite Retrievals in a Terrestrial Biosphere Model Using a Process-Based SIF Model. *Journal of Geophysical Research: Biogeosciences*, *124*(11), 3281–3306. https://doi.org/10.1029/2019JG005040

Bandhauer. (2021). Evaluation of daily precipitation analyses in E-OBS (v19.0e) and ERA5

by comparison to regional high-resolution datasets in European regions. *International Journal of Climatology*, *42*, 727–747. https://doi.org/DOI: 10.1002/joc.7269

Bastos, A., Orth, R., Reichstein, M., Ciais, P., Viovy, N., Zaehle, S., Anthoni, P., Arneth, A., Gentine, P., Joetzjer, E., Lienert, S., Loughran, T., McGuire, P. C., Sungmin, O., Pongratz, J., & Sitch, S. (2021). Vulnerability of European ecosystems to two compound dry and hot summers in 2018 and 2019. *Earth System Dynamics*, *12*(4), 1015–1035. https://doi.org/10.5194/esd-12-1015-2021

Bugmann, H., & Seidl, R. (2022). The evolution, complexity and diversity of models of long-term forest dynamics. *Journal of Ecology*, *110*(10), 2288–2307. https://doi.org/10.1111/1365-2745.13989

Butterfield, Z., Buermann, W., & Keppel-Aleks, G. (2020). Satellite observations reveal seasonal redistribution of northern ecosystem productivity in response to interannual climate variability. *Remote Sensing of Environment*, *242*(June 2019). https://doi.org/10.1016/j.rse.2020.111755

Carvalhais, N., Reichstein, M., Ciais, P., Collatz, G. J., Mahecha, M. D., Montagnani, L., Papale, D., Rambal, S., & Seixas, J. (2010). Identification of vegetation and soil carbon pools out of equilibrium in a process model via eddy covariance and biometric constraints. *Global Change Biology*, *16*(10), 2813–2829. https://doi.org/10.1111/j.1365-2486.2010.02173.x

Carvalhais, N., Reichstein, M., Seixas, J., Colltaz, G. J., Pereira, J. S., Berbigier, P., Carrara, A., Granier, A., Montagnani, L., Papale, D., Rambal, S., Sanz, M. J., & Valentini, R. (2008). Implications of the carbon cycle steady state assumption for biogeochemical modeling performance and inverse parameter retrieval. *Global Biogeochemical Cycles*, *22*(2), 1–16. https://doi.org/10.1029/2007GB003033

Castellaneta, M., Rita, A., Camarero, J. J., Colangelo, M., & Ripullone, F. (2022). Declines in canopy greenness and tree growth are caused by combined climate extremes during drought-induced dieback. *Science of the Total Environment*, *813*, 152666. https://doi.org/10.1016/j.scitotenv.2021.152666

Chen, A., Mao, J., Ricciuto, D., Lu, D., Xiao, J., Li, X., Thornton, P. E., & Knapp, A. K. (2021). Seasonal changes in GPP/SIF ratios and their climatic determinants across the Northern Hemisphere. *Global Change Biology*, *27*(20), 5186–5197. https://doi.org/10.1111/gcb.15775

Chen, L., Keski-Saari, S., Kontunen-Soppela, S., Zhu, X., Zhou, X., Hänninen, H., Pumpanen, J., Mola-Yudego, B., Wu, D., & Berninger, F. (2023a). Immediate and carry-over effects of late-spring frost and growing season drought on forest gross primary productivity capacity in the Northern Hemisphere. *Global Change Biology*, *October 2022*, 1–17. https://doi.org/10.1111/gcb.16751

Chen, L., Keski-Saari, S., Kontunen-Soppela, S., Zhu, X., Zhou, X., Hänninen, H., Pumpanen, J., Mola-Yudego, B., Wu, D., & Berninger, F. (2023b). Immediate and carry-over effects of late-spring frost and growing season drought on forest gross primary productivity capacity in the Northern Hemisphere. *Global Change Biology*, *March*, 1–17. https://doi.org/10.1111/gcb.16751

Chiesi, M., Fibbi, L., Genesio, L., Gioli, B., Magno, R., Maselli, F., Moriondo, M., & Vaccari, F. P. (2011). Integration of ground and satellite data to model Mediterranean forest processes. *International Journal of Applied Earth Observation and Geoinformation*, *13*(3), 504–515. https://doi.org/10.1016/j.jag.2010.10.006

Chiesi, M., Moriondo, M., Maselli, F., Gardin, L., Fibbi, L., Bindi, M., & Running, S. W. (2010). Simulation of mediterranean forest carbon pools under expected environmental scenarios. *Canadian Journal of Forest Research*, *40*(5), 850–860. https://doi.org/10.1139/X10-037

Chirici, G., Giannetti, F., McRoberts, R. E., Travaglini, D., Pecchi, M., Maselli, F., Chiesi, M., & Corona, P. (2020). Wall-to-wall spatial prediction of growing stock volume based on Italian National Forest Inventory plots and remotely sensed data. *International Journal of Applied Earth Observation and Geoinformation*, *84*(September 2019). https://doi.org/10.1016/j.jag.2019.101959

Collalti, A., Marconi, S., Ibrom, A., Trotta, C., Anav, A., D'andrea, E., Matteucci, G., Montagnani, L., Gielen, B., Mammarella, I., Grünwald, T., Knohl, A., Berninger, F., Zhao, Y., Valentini, R., & Santini, M. (2016). Validation of 3D-CMCC Forest Ecosystem Model (v.5.1) against eddy covariance data for 10 European forest sites. *Geoscientific Model Development*, *9*(2), 479–504. https://doi.org/10.5194/gmd-9-479-2016

Collalti, A., Perugini, L., Santini, M., Chiti, T., Nolè, A., Matteucci, G., & Valentini, R. (2014). A process-based model to simulate growth in forests with complex structure: Evaluation and use of 3D-CMCC Forest Ecosystem Model in a deciduous forest in Central Italy. *Ecological Modelling*, *272*, 362–378. https://doi.org/10.1016/j.ecolmodel.2013.09.016

Collalti, A., Thornton, P. E., Cescatti, A., Rita, A., Borghetti, M., Nolè, A., Trotta, C., Ciais, P., & Matteucci, G. (2019). The sensitivity of the forest carbon budget shifts across processes along with stand development and climate change. *Ecological Applications*, *29*(2), 1–18. https://doi.org/10.1002/eap.1837

Collalti, A., Trotta, C., Keenan, T. F., Ibrom, A., Bond-Lamberty, B., Grote, R., Vicca, S., Reyer, C. P. O., Migliavacca, M., Veroustraete, F., Anav, A., Campioli, M., Scoccimarro, E., Šigut, L., Grieco, E., Cescatti, A., & Matteucci, G. (2018). Thinning Can Reduce Losses in Carbon Use Efficiency and Carbon Stocks in Managed Forests Under Warmer Climate. *Journal of Advances in Modeling Earth Systems*, *10*(10), 2427–2452. https://doi.org/10.1029/2018MS001275

Cornes, R. C., van der Schrier, G., van den Besselaar, E. J. M., & Jones, P. D. (2018). An Ensemble Version of the E-OBS Temperature and Precipitation Data Sets. *Journal of Geophysical Research: Atmospheres*, *123*(17), 9391–9409. https://doi.org/10.1029/2017JD028200

Corona, P. (2008). La carta forestale della Toscana. *Forest@ - Rivista Di Selvicoltura Ed Ecologia Forestale*, *3*(3), 41.

Crow, W. T., Gomez, C. A., Sabater, J. M., Holmes, T., Hain, C. R., Lei, F., Dong, J., Alfieri, J. G., & Anderson, M. C. (2020). Soil moisture–evapotranspiration overcoupling and l-band brightness temperature assimilation: Sources and forecast implications. *Journal of Hydrometeorology*, *21*(10), 2359–2374. https://doi.org/10.1175/JHM-D-20-0088.1

D'Andrea, E., Rezaie, N., Prislan, P., Gričar, J., Collalti, A., Muhr, J., & Matteucci, G. (2020). Frost and drought: Effects of extreme weather events on stem carbon dynamics in a Mediterranean beech forest. *Plant Cell and Environment*, *43*(10), 2365–2379. https://doi.org/10.1111/pce.13858

D'Andrea, E., Scartazza, A., Battistelli, A., Collalti, A., Proietti, S., Rezaie, N., Matteucci, G., & Moscatello, S. (2021). Unravelling resilience mechanisms in forests: role of non-structural carbohydrates in responding to extreme weather events. *Tree Physiology*,

41(10), 1808–1818. https://doi.org/10.1093/treephys/tpab044

Dalmonech, D., Marano, G., Amthor, J. S., Cescatti, A., Lindner, M., Trotta, C., & Collalti, A. (2022). Feasibility of enhancing carbon sequestration and stock capacity in temperate and boreal European forests via changes to management regimes. *Agricultural and Forest Meteorology*, *327*(April), 109203. https://doi.org/10.1016/j.agrformet.2022.109203

Dosio, A., & Paruolo, P. (2011). Bias correction of the ENSEMBLES high-resolution climate change projections for use by impact models: Evaluation on the present climate. *Journal of Geophysical Research Atmospheres*, *116*(16), 1–22. https://doi.org/10.1029/2011JD015934

Dubrovský, M., Hayes, M., Duce, P., Trnka, M., Svoboda, M., & Zara, P. (2014). Multi-GCM projections of future drought and climate variability indicators for the Mediterranean region. *Regional Environmental Change*, *14*(5), 1907–1919. https://doi.org/10.1007/s10113-013-0562-z

Fan, Y., Miguez-Macho, G., Jobbágy, E. G., Jackson, R. B., & Otero-Casal, C. (2017). Hydrologic regulation of plant rooting depth. *Proceedings of the National Academy of Sciences of the United States of America*, *114*(40), 10572–10577. https://doi.org/10.1073/pnas.1712381114

Fang, J., & Lechowicz, M. J. (2006). Climatic limits for the present distribution of beech (Fagus L.) species in the world. *Journal of Biogeography*, *33*(10), 1804–1819. https://doi.org/10.1111/j.1365-2699.2006.01533.x

Fang, Y., Leung, L. R., Wolfe, B. T., Detto, M., Knox, R. G., McDowell, N. G., Grossiord, C., Xu, C., Christoffersen, B. O., Gentine, P., Koven, C. D., & Chambers, J. Q. (2021). Disentangling the Effects of Vapor Pressure Deficit and Soil Water Availability on Canopy Conductance in a Seasonal Tropical Forest During the 2015 El Niño Drought. *Journal of Geophysical Research: Atmospheres*, *126*(10), 1–20. https://doi.org/10.1029/2021JD035004

Fernández-Martínez, M., Peñuelas, J., Chevallier, F., Ciais, P., Obersteiner, M., Rödenbeck, C., Sardans, J., Vicca, S., Yang, H., Sitch, S., Friedlingstein, P., Arora, V. K., Goll, D. S., Jain, A. K., Lombardozzi, D. L., McGuire, P. C., & Janssens, I. A. (2023). Diagnosing destabilization risk in global land carbon sinks. *Nature*, *615*(November 2021). https://doi.org/10.1038/s41586-023-05725-1

Fibbi, L., Chiesi, M., Moriondo, M., Bindi, M., Chirici, G., Papale, D., Gozzini, B., & Maselli, F. (2016). Correction of a 1 km daily rainfall dataset for modelling forest ecosystem processes in Italy. *Meteorological Applications*, *23*(2), 294–303. https://doi.org/10.1002/met.1554

Francini, S., McRoberts, R. E., Giannetti, F., Marchetti, M., Scarascia Mugnozza, G., & Chirici, G. (2021). The Three Indices Three Dimensions (3I3D) algorithm: a new method for forest disturbance mapping and area estimation based on optical remotely sensed imagery. *International Journal of Remote Sensing*, *42*(12), 4697–4715. https://doi.org/10.1080/01431161.2021.1899334

Gauquelin, T., Michon, G., Joffre, R., Duponnois, R., Génin, D., Fady, B., Bou Dagher-Kharrat, M., Derridj, A., Slimani, S., Badri, W., Alifriqui, M., Auclair, L., Simenel, R., Aderghal, M., Baudoin, E., Galiana, A., Prin, Y., Sanguin, H., Fernandez, C., & Baldy, V. (2018). Mediterranean forests, land use and climate change: a social-ecological perspective. *Regional Environmental Change*, *18*(3), 623–636. https://doi.org/10.1007/s10113-016-0994-3

Giannetti, F., Chirici, G., Vangi, E., Corona, P., Maselli, F., Chiesi, M., D'Amico, G., & Puletti, N. (2022). Wall-to-Wall Mapping of Forest Biomass and Wood Volume Increment in Italy. *Forests*, *13*(12). https://doi.org/10.3390/f13121989

Grossiord, C., Buckley, T. N., Cernusak, L. A., Novick, K. A., Poulter, B., Siegwolf, R. T. W., Sperry, J. S., & McDowell, N. G. (2020). Plant responses to rising vapor pressure deficit. *New Phytologist*, *226*(6), 1550–1566. https://doi.org/10.1111/nph.16485

Grünig, M., Seidl, R., & Senf, C. (2023). Increasing aridity causes larger and more severe forest fires across Europe. *Global Change Biology*, *29*(6), 1648–1659. https://doi.org/10.1111/gcb.16547

Gutsch, M., Lasch-Born, P., Kollas, C., Suckow, F., & Reyer, C. P. O. (2018). Balancing trade-offs between ecosystem services in Germany's forests under climate change. *Environmental Research Letters*, *13*(4). https://doi.org/10.1088/1748-9326/aab4e5

Hanson, P. J., Amthor, J. S., Wullschleger, S. D., Wilson, K. B., Grant, R. F., Hartley, A., Hui, D., Hunt, E. R., Johnson, D. W., Kimball, J. S., King, A. W., Luo, Y., McNulty, S. G., Sun, G., Thornton, P. E., Wang, S., Williams, M., Baldocchi, D. D., & Cushman, R. M. (2004). Oak forest carbon and water simulations: Model intercomparisons and evaluations against independent data. *Ecological Monographs*, *74*(3), 443–489. https://doi.org/10.1890/03-4049

Härkönen, S., Neumann, M., Mues, V., Berninger, F., Bronisz, K., Cardellini, G., Chirici, G., Hasenauer, H., Koehl, M., Lang, M., Merganicova, K., Mohren, F., Moiseyev, A., Moreno, A., Mura, M., Muys, B., Olschofsky, K., Del Perugia, B., Rørstad, P. K., … Mäkelä, A. (2019). A climate-sensitive forest model for assessing impacts of forest management in Europe. *Environmental Modelling and Software*, *115*(February), 128–143. https://doi.org/10.1016/j.envsoft.2019.02.009

Haylock, M. R., Hofstra, N., Klein Tank, A. M. G., Klok, E. J., Jones, P. D., & New, M. (2008). A European daily high-resolution gridded data set of surface temperature and precipitation for 1950-2006. *Journal of Geophysical Research Atmospheres*, *113*(20), 1–12. https://doi.org/10.1029/2008JD010201

Herrera, S., Margarida Cardoso, R., Matos Soares, P., Espírito-Santo, F., Viterbo, P., & Gutiérrez, J. M. (2019). Iberia01: A new gridded dataset of daily precipitation and temperatures over Iberia. *Earth System Science Data*, *11*(4), 1947–1956. https://doi.org/10.5194/essd-11-1947-2019

Hiederer, R. (2013). Mapping Soil Properties for Europe - Spatial Representation of Soil Database Attributes. In *JRC Technical Reports*. http://scholar.google.com/scholar?hl=en&btnG=Search&q=intitle:Mapping+Soil+Properties+for+Europe+-+Spatial+Representation+of+Soil+Database+Attributes#0

Hijmans, R. J., Bivand, R., Forner, K., Ooms, J., Pebesma, E., & Sumner, M. D. (2022). *Package ' terra .' 3*(500), 1–6.

Janssen, P. H. M., & Heuberger, P. S. C. (1995). Calibration of process-oriented models. *Ecological Modelling*, *83*(1–2), 55–66. https://doi.org/10.1016/0304-3800(95)00084-9

Jung, M., Koirala, S., Weber, U., Ichii, K., Gans, F., Camps-Valls, G., Papale, D., Schwalm, C., Tramontana, G., & Reichstein, M. (2019). The FLUXCOM ensemble of global land-atmosphere energy fluxes. *Scientific Data*, *6*(1), 1–14. https://doi.org/10.1038/s41597-019-0076-8

Jung, M., Schwalm, C., Migliavacca, M., Walther, S., Camps-Valls, G., Koirala, S., Anthoni, P., Besnard, S., Bodesheim, P., Carvalhais, N., Chevallier, F., Gans, F., S Goll, D.,

Haverd, V., Köhler, P., Ichii, K., K Jain, A., Liu, J., Lombardozzi, D., … Reichstein, M. (2020). Scaling carbon fluxes from eddy covariance sites to globe: Synthesis and evaluation of the FLUXCOM approach. *Biogeosciences*, *17*(5), 1343–1365. https://doi.org/10.5194/bg-17-1343-2020

Kannenberg, S. A., Schwalm, C. R., & Anderegg, W. R. L. (2020). Ghosts of the past: how drought legacy effects shape forest functioning and carbon cycling. *Ecology Letters*, *23*(5), 891–901. https://doi.org/10.1111/ele.13485

Koch, J., Demirel, M. C., & Stisen, S. (2018). The SPAtial EFficiency metric (SPAEF): Multiple-component evaluation of spatial patterns for optimization of hydrological models. *Geoscientific Model Development*, *11*(5), 1873–1886. https://doi.org/10.5194/gmd-11-1873-2018

Kollet, S. J., & Maxwell, R. M. (2008). Capturing the influence of groundwater dynamics on land surface processes using an integrated, distributed watershed model. *Water Resources Research*, *44*(2), 1–18. https://doi.org/10.1029/2007WR006004

Kumar, S. V., Peters-Lidard, C. D., Mocko, D., Reichle, R., Liu, Y., Arsenault, K. R., Xia, Y., Ek, M., Riggs, G., Livneh, B., & Cosh, M. (2014). Assimilation of remotely sensed soil moisture and snow depth retrievals for drought estimation. *Journal of Hydrometeorology*, *15*(6), 2446–2469. https://doi.org/10.1175/JHM-D-13-0132.1

Li, X., & Xiao, J. (2019a). A global, 0.05-degree product of solar-induced chlorophyll fluorescence derived from OCO-2, MODIS, and reanalysis data. *Remote Sensing*, *11*(5). https://doi.org/10.3390/rs11050517

Li, X., & Xiao, J. (2019b). Mapping photosynthesis solely from solar-induced chlorophyll fluorescence: A global, fine-resolution dataset of gross primary production derived from OCO-2. *Remote Sensing*, *11*(21). https://doi.org/10.3390/rs11212563

Li, X., Xiao, J., He, B., Altaf Arain, M., Beringer, J., Desai, A. R., Emmel, C., Hollinger, D. Y., Krasnova, A., Mammarella, I., Noe, S. M., Ortiz, P. S., Rey-Sanchez, A. C., Rocha, A. V., & Varlagin, A. (2018). Solar-induced chlorophyll fluorescence is strongly correlated with terrestrial photosynthesis for a wide variety of biomes: First global analysis based on OCO-2 and flux tower observations. *Global Change Biology*, *24*(9), 3990–4008. https://doi.org/10.1111/gcb.14297

Liaw, A., & Wiener, M. (2002). Classification and Regression by randomForest. *R News*, *2*(3), 18–22.

Lindeskog, M., Smith, B., Lagergren, F., Sycheva, E., Ficko, A., Pretzsch, H., & Rammig, A. (2021). Accounting for forest management in the estimation of forest carbon balance using the dynamic vegetation model LPJ-GUESS (v4.0, r9710): Implementation and evaluation of simulations for Europe. *Geoscientific Model Development*, *14*(10), 6071–6112. https://doi.org/10.5194/gmd-14-6071-2021

Lorenz, R., Stalhandske, Z., & Fischer, E. M. (2019). Detection of a Climate Change Signal in Extreme Heat, Heat Stress, and Cold in Europe From Observations. *Geophysical Research Letters*, *46*(14), 8363–8374. https://doi.org/10.1029/2019GL082062

Mahnken, M., Cailleret, M., Collalti, A., Trotta, C., Biondo, C., D'Andrea, E., Dalmonech, D., Marano, G., Mäkelä, A., Minunno, F., Peltoniemi, M., Trotsiuk, V., Nadal-Sala, D., Sabaté, S., Vallet, P., Aussenac, R., Cameron, D. R., Bohn, F. J., Grote, R., … Reyer, C. P. O. (2022). Accuracy, realism and general applicability of European forest models. *Global Change Biology*, *28*(23), 6921–6943. https://doi.org/10.1111/gcb.16384

Marchand, W., Buechling, A., Rydval, M., Čada, V., Stegehuis, A. I., Fruleux, A., Poláček,

M., Hofmeister, J., Pavlin, J., Ralhan, D., Dušátko, M., Janda, P., Mikoláš, M., Vostarek, O., Bače, R., Frankovič, M., Kozák, D., Roibu, C. C., Chaskovskyy, O., … Svoboda, M. (2023). Accelerated growth rates of Norway spruce and European beech saplings from Europe's temperate primary forests are related to warmer conditions. *Agricultural and Forest Meteorology*, *329*(March 2022). https://doi.org/10.1016/j.agrformet.2022.109280

Marconi, S., Chiti, T., Nolè, A., Valentini, R., & Collalti, A. (2017). The role of respiration in estimation of net carbon cycle: Coupling soil carbon dynamics and canopy turnover in a novel version of 3D-CMCC forest ecosystem model. *Forests*, *8*(6). https://doi.org/10.3390/f8060220

Maréchaux, I., Langerwisch, F., Huth, A., Bugmann, H., Morin, X., Reyer, C. P. O., Seidl, R., Collalti, A., Dantas de Paula, M., Fischer, R., Gutsch, M., Lexer, M. J., Lischke, H., Rammig, A., Rödig, E., Sakschewski, B., Taubert, F., Thonicke, K., Vacchiano, G., & Bohn, F. J. (2021). Tackling unresolved questions in forest ecology: The past and future role of simulation models. *Ecology and Evolution*, *11*(9), 3746–3770. https://doi.org/10.1002/ece3.7391

Maselli, F., Argenti, G., Chiesi, M., Angeli, L., & Papale, D. (2013). Simulation of grassland productivity by the combination of ground and satellite data. *Agriculture, Ecosystems and Environment*, *165*, 163–172. https://doi.org/10.1016/j.agee.2012.11.006

Maselli, F., Barbati, A., Chiesi, M., Chirici, G., & Corona, P. (2006). Use of remotely sensed and ancillary data for estimating forest gross primary productivity in Italy. *Remote Sensing of Environment*, *100*(4), 563–575. https://doi.org/10.1016/j.rse.2005.11.010

Maselli, F., Papale, D., Puletti, N., Chirici, G., & Corona, P. (2009). Combining remote sensing and ancillary data to monitor the gross productivity of water-limited forest ecosystems. *Remote Sensing of Environment*, *113*(3), 657–667. https://doi.org/10.1016/j.rse.2008.11.008

Maselli, F., Pasqui, M., Chirici, G., Chiesi, M., Fibbi, L., Salvati, R., & Corona, P. (2012). Modeling primary production using a 1 km daily meteorological data set. *Climate Research*, *54*(3), 271–285. https://doi.org/10.3354/cr01121

Massari, C., Brocca, L., Pellarin, T., Abramowitz, G., Filippucci, P., Ciabatta, L., Maggioni, V., Kerr, Y., & Fernandez Prieto, D. (2020). A daily 25 km short-latency rainfall product for data-scarce regions based on the integration of the Global Precipitation Measurement mission rainfall and multiple-satellite soil moisture products. *Hydrology and Earth System Sciences*, *24*(5), 2687–2710. https://doi.org/10.5194/hess-24-2687-2020

Médail, F., Monnet, A. C., Pavon, D., Nikolic, T., Dimopoulos, P., Bacchetta, G., Arroyo, J., Barina, Z., Albassatneh, M. C., Domina, G., Fady, B., Matevski, V., Mifsud, S., & Leriche, A. (2019). What is a tree in the mediterranean basin hotspot? A critical analysis. *Forest Ecosystems*, *6*(1). https://doi.org/10.1186/s40663-019-0170-6

Minunno, F., Peltoniemi, M., Härkönen, S., Kalliokoski, T., Makinen, H., & Mäkelä, A. (2019). Bayesian calibration of a carbon balance model PREBAS using data from permanent growth experiments and national forest inventory. *Forest Ecology and Management*, *440*(March), 208–257. https://doi.org/10.1016/j.foreco.2019.02.041

Moreno, A., & Hasenauer, H. (2016). Spatial downscaling of European climate data. *International Journal of Climatology*, *36*(3), 1444–1458. https://doi.org/10.1002/joc.4436

Niu, G. Y., Yang, Z. L., Mitchell, K. E., Chen, F., Ek, M. B., Barlage, M., Kumar, A.,

Manning, K., Niyogi, D., Rosero, E., Tewari, M., & Xia, Y. (2011). The community Noah land surface model with multiparameterization options (Noah-MP): 1. Model description and evaluation with local-scale measurements. *Journal of Geophysical Research Atmospheres*, *116*(12), 1–19. https://doi.org/10.1029/2010JD015139

Noce, S., Collalti, A., Valentini, R., & Santini, M. (2016). Hot spot maps of forest presence in the Mediterranean basin. *IForest*, *9*(5), 766–774. https://doi.org/10.3832/ifor1802-009

Norton, A. J., Rayner, P. J., Koffi, E. N., Scholze, M., Silver, J. D., & Wang, Y. P. (2019). Estimating global gross primary productivity using chlorophyll fluorescence and a data assimilation system with the BETHY-SCOPE model. *Biogeosciences*, *16*(15), 3069–3093. https://doi.org/10.5194/bg-16-3069-2019

Noto, L. V., Cipolla, G., Francipane, A., & Pumo, D. (2022). Climate Change in the Mediterranean Basin (Part I): Induced Alterations on Climate Forcings and Hydrological Processes. *Water Resources Management*, 2287–2305. https://doi.org/10.1007/s11269-022-03400-0

O'Sullivan, M., Smith, W. K., Sitch, S., Friedlingstein, P., Arora, V. K., Haverd, V., Jain, A. K., Kato, E., Kautz, M., Lombardozzi, D., Nabel, J. E. M. S., Tian, H., Vuichard, N., Wiltshire, A., Zhu, D., & Buermann, W. (2020). Climate-Driven Variability and Trends in Plant Productivity Over Recent Decades Based on Three Global Products. *Global Biogeochemical Cycles*, *34*(12). https://doi.org/10.1029/2020GB006613

Pastorello, G., Trotta, C., Canfora, E., Chu, H., Christianson, D., Cheah, Y. W., Poindexter, C., Chen, J., Elbashandy, A., Humphrey, M., Isaac, P., Polidori, D., Ribeca, A., van Ingen, C., Zhang, L., Amiro, B., Ammann, C., Arain, M. A., Ardö, J., … Papale, D. (2020). The FLUXNET2015 dataset and the ONEFlux processing pipeline for eddy covariance data. *Scientific Data*, *7*(1), 225. https://doi.org/10.1038/s41597-020-0534-3

Patacca, M., Lindner, M., Lucas-Borja, M. E., Cordonnier, T., Fidej, G., Gardiner, B., Hauf, Y., Jasinevičius, G., Labonne, S., Linkevičius, E., Mahnken, M., Milanovic, S., Nabuurs, G. J., Nagel, T. A., Nikinmaa, L., Panyatov, M., Bercak, R., Seidl, R., Ostrogović Sever, M. Z., … Schelhaas, M. J. (2023). Significant increase in natural disturbance impacts on European forests since 1950. *Global Change Biology*, *29*(5), 1359–1376. https://doi.org/10.1111/gcb.16531

Peano, D., Materia, S., Collalti, A., Alessandri, A., Anav, A., Bombelli, A., & Gualdi, S. (2019). Global Variability of Simulated and Observed Vegetation Growing Season. *Journal of Geophysical Research: Biogeosciences*, *124*(11), 3569–3587. https://doi.org/10.1029/2018JG004881

Peaucelle, M., Janssens, I. A., Stocker, B. D., Descals Ferrando, A., Fu, Y. H., Molowny-Horas, R., Ciais, P., & Peñuelas, J. (2019). Spatial variance of spring phenology in temperate deciduous forests is constrained by background climatic conditions. *Nature Communications*, *10*(1), 1–10. https://doi.org/10.1038/s41467-019-13365-1

Peñuelas, J., Sardans, J., Filella, I., Estiarte, M., Llusià, J., Ogaya, R., Carnicer, J., Bartrons, M., Rivas-Ubach, A., Grau, O., Peguero, G., Margalef, O., Pla-Rabés, S., Stefanescu, C., Asensio, D., Preece, C., Liu, L., Verger, A., Barbeta, A., … Terradas, J. (2017). Impacts of global change on Mediterranean forests and their services. *Forests*, *8*(12), 1–37. https://doi.org/10.3390/f8120463

Pretzsch, H., Grote, R., Reineking, B., Rötzer, T., & Seifert, S. (2008). Models for forest ecosystem management: A European perspective. *Annals of Botany*, *101*(8), 1065–1087. https://doi.org/10.1093/aob/mcm246

Qiu, R., Han, G., Ma, X., Xu, H., Shi, T., & Zhang, M. (2020). A comparison of OCO-2 SIF, MODIS GPP, and GOSIF data from gross primary production (GPP) estimation and seasonal cycles in North America. *Remote Sensing*, *12*(2). https://doi.org/10.3390/rs12020258

Reyer, C. (2015). Forest productivity under environmental change—A review of stand-scale modeling studies. *Current Forestry Reports*, *1*(2), 53–68. https://doi.org/10.1007/s40725-015-0009-5

Reyer, C., Lasch-Born, P., Suckow, F., Gutsch, M., Murawski, A., & Pilz, T. (2014). Projections of regional changes in forest net primary productivity for different tree species in Europe driven by climate change and carbon dioxide. *Annals of Forest Science*, *71*(2), 211–225. https://doi.org/10.1007/s13595-013-0306-8

Reyer, C. P. O., Silveyra Gonzalez, R., Dolos, K., Hartig, F., Hauf, Y., Noack, M., Lasch-Born, P., Rötzer, T., Pretzsch, H., Meesenburg, H., Fleck, S., Wagner, M., Bolte, A., Sanders, T. G. M., Kolari, P., Mäkelä, A., Vesala, T., Mammarella, I., Pumpanen, J., … Frieler, K. (2020). The PROFOUND Database for evaluating vegetation models and simulating climate impacts on European forests. *Earth System Science Data*, *12*(2), 1295–1320. https://doi.org/10.5194/essd-12-1295-2020

Richards, F. J. (1959). A flexible growth function for empirical use. *Journal of Experimental Botany*, *10*(2), 290–301. https://doi.org/10.1093/jxb/10.2.290

Ripullone, F., Camarero, J. J., Colangelo, M., & Voltas, J. (2020). Variation in the access to deep soil water pools explains tree-to-tree differences in drought-triggered dieback of mediterranean oaks. *Tree Physiology*, *40*(5), 591–604. https://doi.org/10.1093/treephys/tpaa026

Rita, A., Camarero, J. J., Nolè, A., Borghetti, M., Brunetti, M., Pergola, N., Serio, C., Vicente-Serrano, S. M., Tramutoli, V., & Ripullone, F. (2020). The impact of drought spells on forests depends on site conditions: The case of 2017 summer heat wave in southern Europe. *Global Change Biology*, *26*(2), 851–863. https://doi.org/10.1111/gcb.14825

Rojas, R., Feyen, L., Dosio, A., & Bavera, D. (2011). Improving pan-European hydrological simulation of extreme events through statistical bias correction of RCM-driven climate simulations. *Hydrology and Earth System Sciences*, *15*(8), 2599–2620. https://doi.org/10.5194/hess-15-2599-2011

S. Tarquini, I. Isola, M. Favalli, F. Mazzarini, M. Bisson, M. T. Pareschi, & E. Boschi. (2009). TINITALY/01: a new Triangular Irregular Network of Italy. *Annals of Geophysics*, *50*(3). https://doi.org/10.4401/ag-4424

Sanchez-Ruiz, S., Chiesi, M., Fibbi, L., Carrara, A., Maselli, F., & Gilabert, M. A. (2018). Optimized Application of Biome-BGC for Modeling the Daily GPP of Natural Vegetation Over Peninsular Spain. *Journal of Geophysical Research: Biogeosciences*, *123*(2), 531–546. https://doi.org/10.1002/2017JG004360

Schenk, H. J., & Jackson, R. B. (2005). Mapping the global distribution of deep roots in relation to climate and soil characteristics. *Geoderma*, *126*(1-2 SPEC. ISS.), 129–140. https://doi.org/10.1016/j.geoderma.2004.11.018

Schuldt, B., Buras, A., Arend, M., Vitasse, Y., Beierkuhnlein, C., Damm, A., Gharun, M., Grams, T. E. E., Hauck, M., Hajek, P., Hartmann, H., Hiltbrunner, E., Hoch, G., Holloway-Phillips, M., Körner, C., Larysch, E., Lübbe, T., Nelson, D. B., Rammig, A., … Kahmen, A. (2020). A first assessment of the impact of the extreme 2018 summer

drought on Central European forests. *Basic and Applied Ecology*, *45*, 86–103. https://doi.org/10.1016/j.baae.2020.04.003

Senf, C., Buras, A., Zang, C. S., Rammig, A., & Seidl, R. (2020). Excess forest mortality is consistently linked to drought across Europe. *Nature Communications*, *11*(1), 1–8. https://doi.org/10.1038/s41467-020-19924-1

Stocker, B. D., Tumber-Dávila, S. J., Konings, A. G., Anderson, M. C., Hain, C., & Jackson, R. B. (2023). Global patterns of water storage in the rooting zones of vegetation. *Nature Geoscience*, *16*(March). https://doi.org/10.1038/s41561-023-01125-2

Suárez-Muñoz, M., Bonet-García, F. J., Navarro-Cerrillo, R., Herrero, J., & Mina, M. (2023). Forest management scenarios drive future dynamics of Mediterranean planted pine forests under climate change. *Landscape Ecology*, *0123456789*. https://doi.org/10.1007/s10980-023-01678-y

Sumner, M., & Hijmans, R. (2023). *Package ' rgdal .'*

Sun, Y., Frankenberg, C., Wood, J. D., Schimel, D. S., Jung, M., Guanter, L., Drewry, D. T., Verma, M., Porcar-Castell, A., Griffis, T. J., Gu, L., Magney, T. S., Köhler, P., Evans, B., & Yuen, K. (2017). OCO-2 advances photosynthesis observation from space via solar-induced chlorophyll fluorescence. *Science*, *358*(6360). https://doi.org/10.1126/science.aam5747

Tedeschi, V., Rey, A., Manca, G., Valentini, R., Jarvis, P. J., & Borghetti, M. (2006). Soil respiration in a Mediterranean oak forest at different developmental stages after coppicing. *Global Change Biology*, *12*(1), 110–121. https://doi.org/10.1111/j.1365-2486.2005.01081.x

Testolin, R., Dalmonech, D., Marano, G., Bagnara, M., D'Andrea, E., Matteucci, G., Noce, S., & Collalti, A. (2023). Simulating diverse forest management options in a changing climate on a Pinus nigra subsp. laricio plantation in Southern Italy. *Science of the Total Environment*, *857*(October 2022), 159361. https://doi.org/10.1016/j.scitotenv.2022.159361

Turco, M., Von Hardenberg, J., AghaKouchak, A., Llasat, M. C., Provenzale, A., & Trigo, R. M. (2017). On the key role of droughts in the dynamics of summer fires in Mediterranean Europe. *Scientific Reports*, *7*(1), 1–10. https://doi.org/10.1038/s41598-017-00116-9

Vangi, E., D'amico, G., Francini, S., Giannetti, F., Lasserre, B., Marchetti, M., McRoberts, R. E., & Chirici, G. (2021). The effect of forest mask quality in the wall-to-wall estimation of growing stock volume. *Remote Sensing*, *13*(5), 1–20. https://doi.org/10.3390/rs13051038

Verkerk, P. J., Delacote, P., Hurmekoski, E., Kunttu, J., Matthews, R., Mäkipää, R., Mosley, F., Perugini, L., Reyer, C. P. O., Roe, S., & Trømborg, E. (2022). *Forest-based climate change mitigation and adaptation in Europe*.

Veroustraete, F., Sabbe, H., & Eerens, H. (2002). Estimation of carbon mass fluxes over Europe using the C-Fix model and Euroflux data. *Remote Sensing of Environment*, *83*(3), 376–399. https://doi.org/10.1016/S0034-4257(02)00043-3

Vicente-Serrano, S. M., Beguería, S., & López-Moreno, J. I. (2010). A multiscalar drought index sensitive to global warming: The standardized precipitation evapotranspiration index. *Journal of Climate*, *23*(7), 1696–1718. https://doi.org/10.1175/2009JCLI2909.1

Wang, S., Zhang, Y., Ju, W., Qiu, B., & Zhang, Z. (2021). Tracking the seasonal and inter-annual variations of global gross primary production during last four decades using

satellite near-infrared reflectance data. *Science of the Total Environment*, *755*. https://doi.org/10.1016/j.scitotenv.2020.142569

Wild, B., Teubner, I., Moesinger, L., Zotta, R., & Forkel, M. (2022). Gross Primary Production Dataset From Microwave Remote Sensing. *Earth System Science Data*, *14*, 1063–1085.

Wohlfahrt, G., Gerdel, K., Migliavacca, M., Rotenberg, E., Tatarinov, F., Müller, J., Hammerle, A., Julitta, T., Spielmann, F. M., & Yakir, D. (2018). Sun-induced fluorescence and gross primary productivity during a heat wave. *Scientific Reports*, *8*(1), 1–9. https://doi.org/10.1038/s41598-018-32602-z

Wu, Z., Ahlström, A., Smith, B., Ardö, J., Eklundh, L., Fensholt, R., & Lehsten, V. (2017). Climate data induced uncertainty in model-based estimations of terrestrial primary productivity. *Environmental Research Letters*, *12*(6). https://doi.org/10.1088/1748-9326/aa6fd8

Xiao, J., Li, X., He, B., Arain, M. A., Beringer, J., Desai, A. R., Emmel, C., Hollinger, D. Y., Krasnova, A., Mammarella, I., Noe, S. M., Serrano Ortiz, P., Rey-Sanchez, C., Rocha, A. V., & Varlagin, A. (2019). Solar-induced chlorophyll fluorescence exhibits a universal relationship with gross primary productivity across a wide variety of biomes. *Global Change Biology*, *25*(4), e4–e6. https://doi.org/10.1111/gcb.14565

Zhang, F., Lu, X., Huang, Q., & Jiang, F. (2022). Impact of different ERA reanalysis data on GPP simulation. *Ecological Informatics*, *68*(August 2021), 101520. https://doi.org/10.1016/j.ecoinf.2021.101520

Zhang, Y., & Ye, A. (2021). Would the obtainable gross primary productivity (GPP) products stand up? A critical assessment of 45 global GPP products. *Science of the Total Environment*, *783*, 146965. https://doi.org/10.1016/j.scitotenv.2021.146965

TABLES

TIME SCALE	METRIC	REFERENCE DATASET		
		GOSIF-GPP	CFIX-GPP	FLUXCOM-GPP
ANNUAL (2005-2013)	R	0.78	0.58	0.67
	β	0.81	1.97	1.10
	γ	0.78	0.84	0.77
				-
MSC (2005-2013)	R^2	0.82	0.91	0.85
IAV-SPRING	R	0.53	/	/
IAV-SUMMER (2005-2019)	R	0.15	/	/

Table 1 | Metrics of the model-reference datasets comparison. MSC: mean seasonal cycle, IAV: interannual variability, RMSE= root mean squared error, FMB= fractional mean bias, R=correlation, β= fraction of the coefficient of variation, γ= model-data histogram intersection metric, R^2 =squared correlation coefficient. For MSC and IAV the median value of the metric is reported.

FIGURES

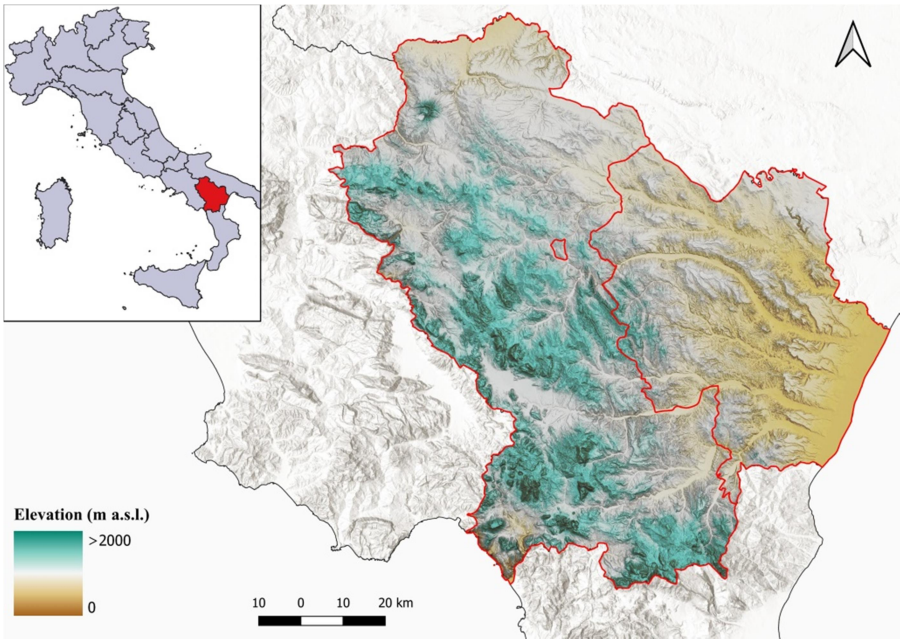

Figure 1 | Location of the study area in the Italian peninsula and elevation map of the Region Basilicata.

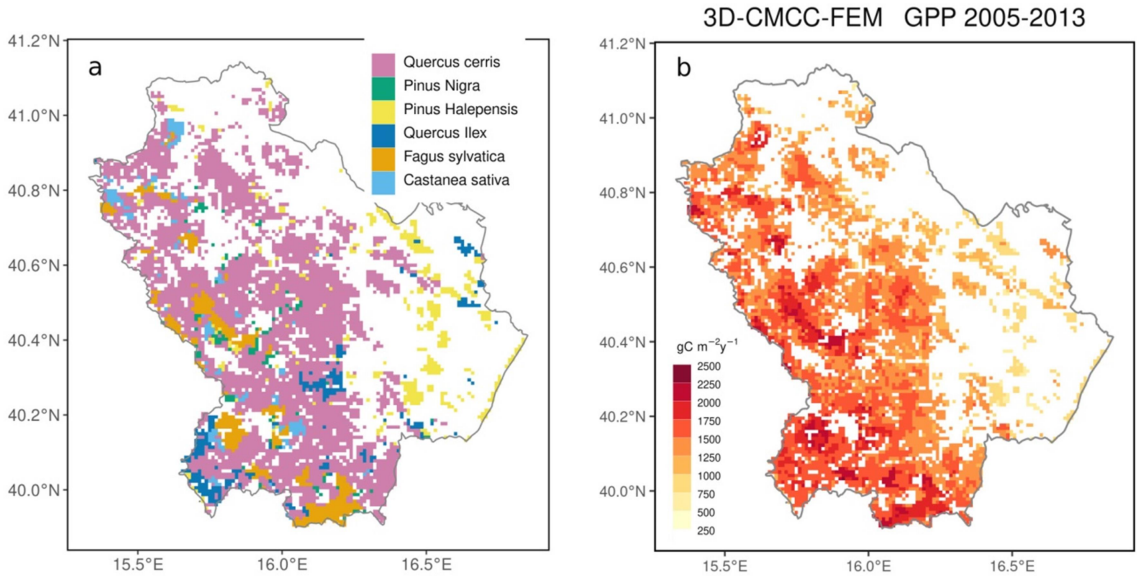

Figure 2 | a) Distribution of the dominant forest class at 1x1 km spatial resolution; b) Modelled multiyear average annual GPP values (gC m^{-2} y^{-1}) for the period 2005-2013 at 1 km resolution. White areas indicate areas not simulated by the model.

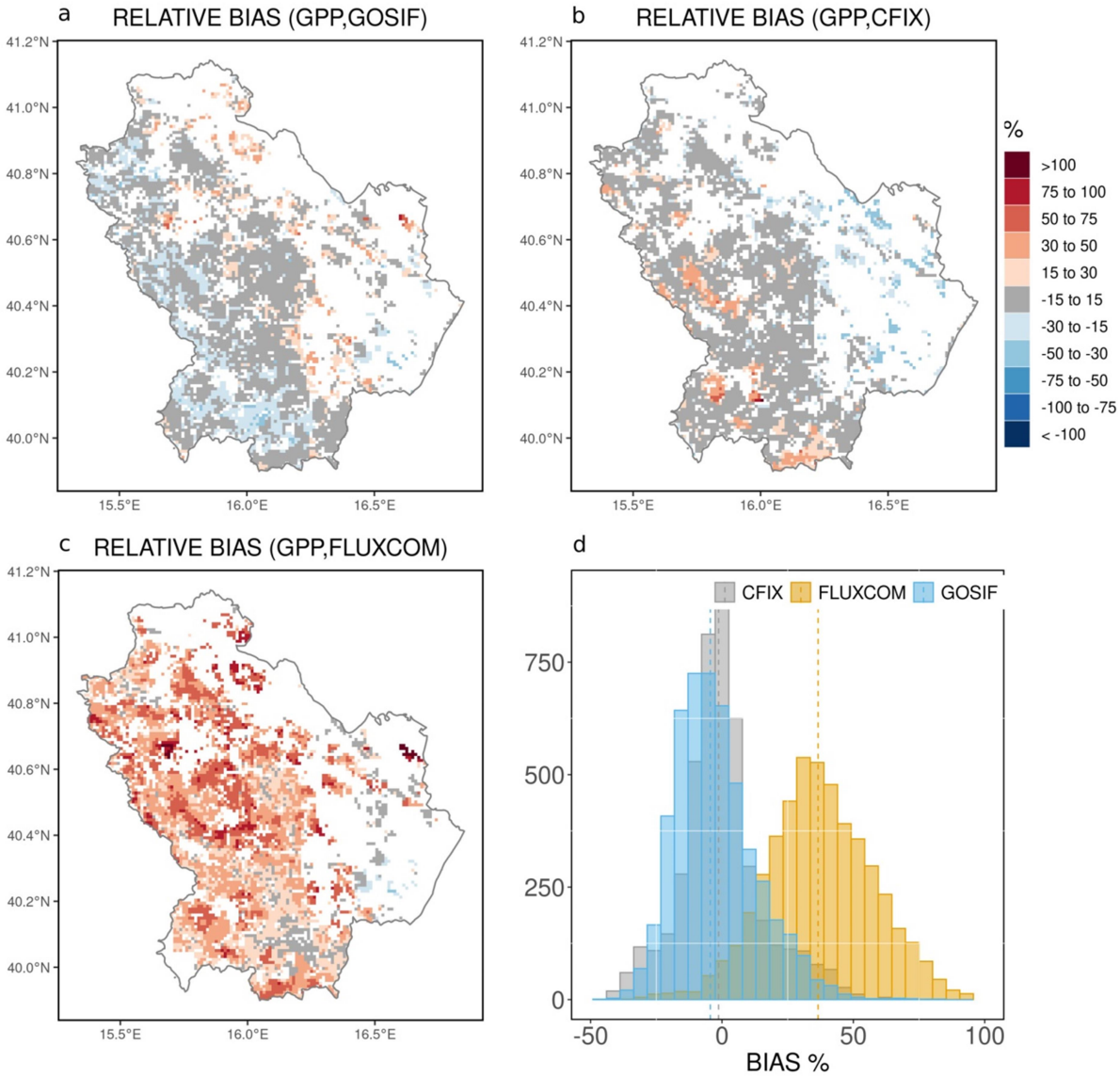

Figure 3 | Spatial distribution of the relative bias defined as (mod-ref)/mod*100, between modeled multiyear mean annual GPP (gC m^{-2} $year^{-1}$) and the satellite-based estimates: a) GOSIF-GPP, b) CFIX-GPP, c) FLUXCOM-GPP; d) histogram of the percentage bias, dashed lines indicate the median value. White areas on the maps indicate areas not simulated by the model. Years of analyses 2005-2013.

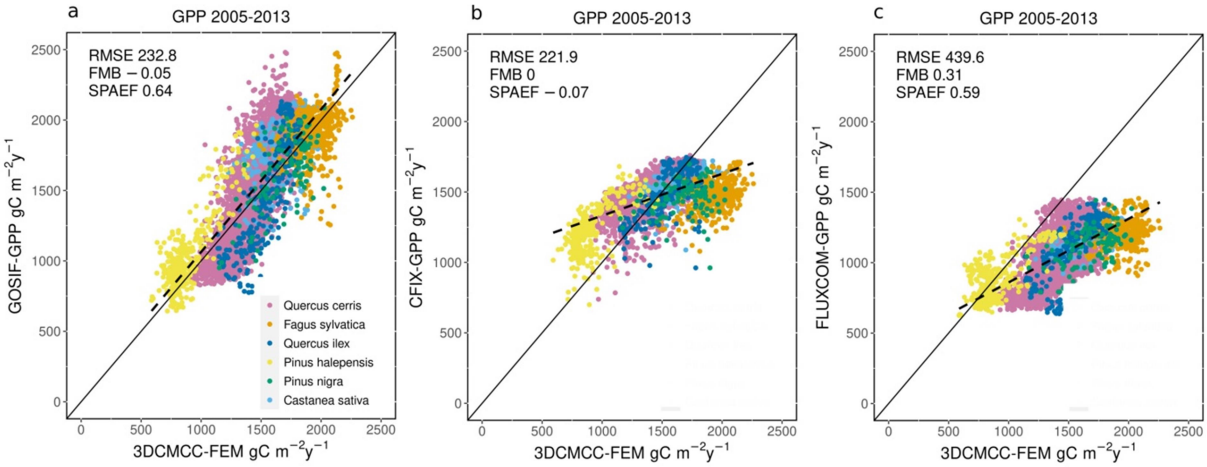

Figure 4 | Model-data scatter plot of the 2005-2013 average annual GPP (gC m^{-2} year^{-1}) simulated by the model and the RS based datasets: a) the GOSIF-GPP b) CFIX-GPP and c) FLUXCOM-GPP estimates (black line is the 1:1 line, dashed line is the linear fit). Each point represents data at grid cell level, different colors indicate the key species considered. RMSE=root mean square error (gC m^{-2} day^{-1}); FMB, fractional bias; SPAEF, spatial efficiency metric.

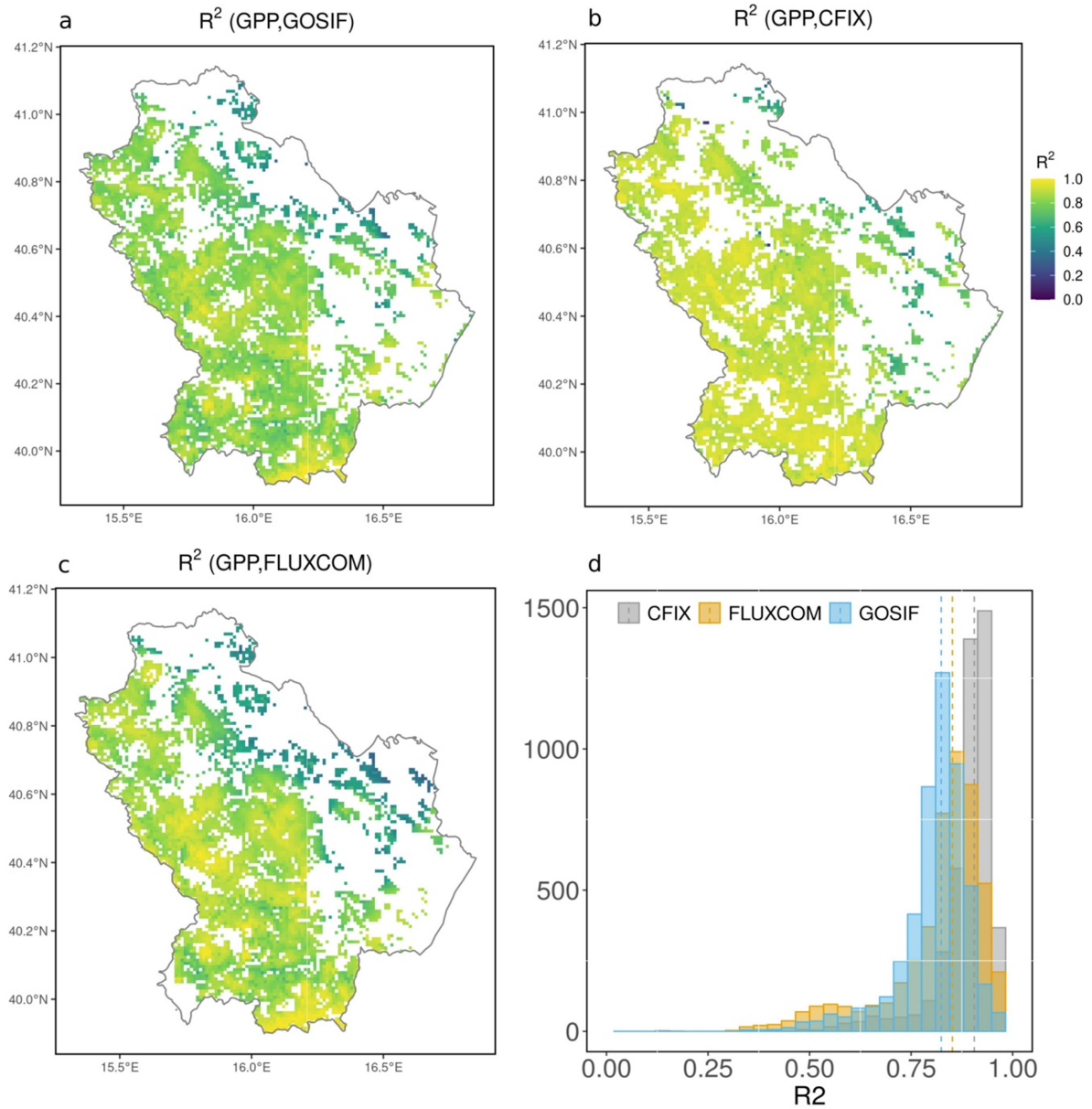

Figure 5 | Spatial coherency of the mean seasonal cycle between model and reference dataset. Shown are grid level squared correlation coefficient R^2 of the 2005-2013 modeled and RS based estimates of: a) GOSIF-GPP, b) CFIX-GPP, c) FLUXCOM-GPP, d) histogram of the R^2, dashed lines indicate the median value. White areas on the maps indicate areas not simulated by the model.

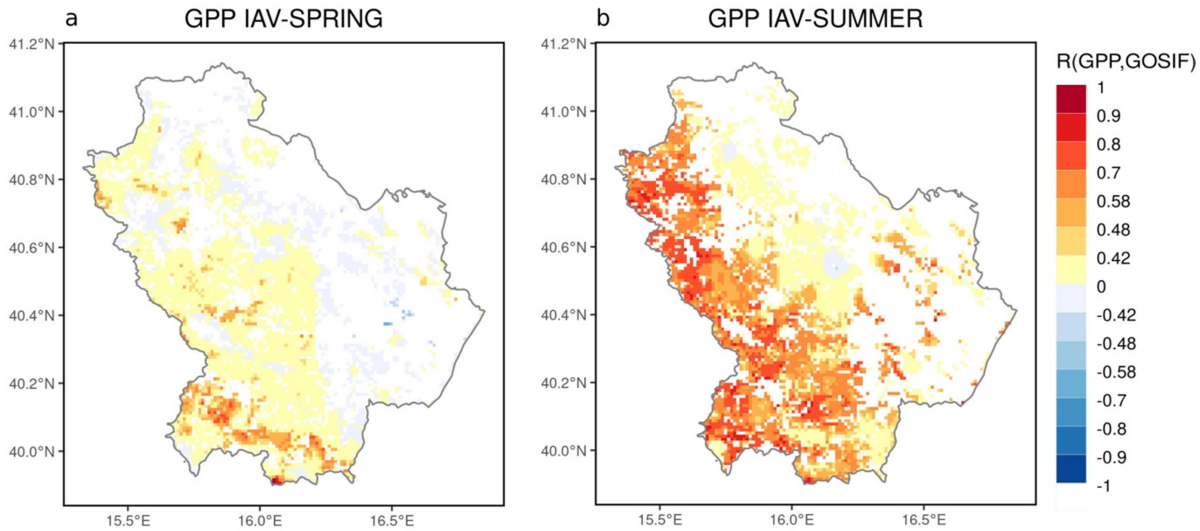

Figure 6 | Coherency of the a) IAV of GPP-spring and b) GPP-summer anomalies between model and RS dataset. Shown are grid level correlation coefficient R of the 2005-2019 modeled and GOSIF-GPP RS estimates of the anomalies. Limits in the color bar indicate the correlation limits for significance: 0.42, P<0.1; 0.48, P<0.05; 0.58 P< 0.01 level. White areas indicate areas not simulated by the model.

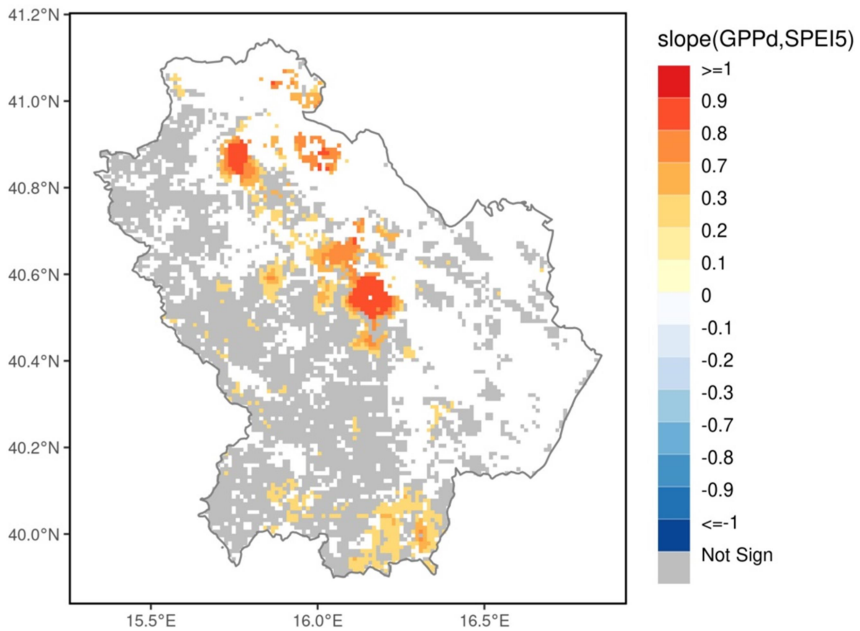

Figure 7 | Spatial distribution of the slope between differences between modeled and GOSIF summer GPP anomalies, GPPd, and SPEI computed at time scale of 5 months, SPEI5, for the years 2005-2019. Grey areas indicate the slope is not significantly different than 0 at P<0.05. White areas on the maps indicate areas not simulated by the model.